

CHAPTER 9

FUNDAMENTALS OF LÉVY FLIGHT PROCESSES

ALEKSEI V. CHECHKIN and VSEVOLOD Y. GONCHAR

*Institute for Theoretical Physics, National Science Center, Kharkov Institute for
Physics and Technology, Kharkov 61108, Ukraine*

JOSEPH KLAFTER

School of Chemistry, Tel Aviv University, 69978 Tel Aviv, Israel

RALF METZLER

*NORDITA—Nordic Institute for Theoretical Physics, DK-2100 Copenhagen Ø,
Denmark*

CONTENTS

- I. Introduction
- II. Definition and Basic Properties of Lévy Flights
 - A. The Langevin Equation with Lévy Noise
 - B. Fractional Fokker–Planck Equation
 - 1. Rescaling of the Dynamical Equations
 - C. Starting Equations in Fourier Space
- III. Confinement and Multimodality
 - A. The Stationary Quartic Cauchy Oscillator
 - B. Power-Law Asymptotics of Stationary Solutions for $c \geq 2$, and Finite Variance for $c > 2$
 - C. Proof of Nonunimodality of Stationary Solution for $c > 2$
 - D. Formal Solution of Equation (38)
 - E. Existence of a Bifurcation Time
 - 1. Trimodal Transient State at $c > 4$
 - 2. Phase Diagrams for n -Modal States
 - F. Consequences
- IV. First Passage and Arrival Time Problems for Lévy Flights
 - A. First Arrival Time
 - B. Sparre Anderson Universality

Fractals, Diffusion, and Relaxation in Disordered Complex Systems: A Special Volume of Advances in Chemical Physics, Volume 133, Part B, edited by William T. Coffey and Yuri P. Kalmykov. Series editor Stuart A. Rice.

Copyright © 2006 John Wiley & Sons, Inc.

- C. Inconsistency of Method of Images
 - V. Barrier Crossing of a Lévy Flight
 - A. Starting Equations
 - B. Brownian Motion
 - C. Numerical Solution
 - D. Analytical Approximation for the Cauchy Case
 - E. Discussion
 - VI. Dissipative Nonlinearity
 - A. Nonlinear Friction Term
 - B. Dynamical Equation with Lévy Noise and Dissipative Nonlinearity
 - C. Asymptotic Behavior
 - D. Numerical Solution of Quadratic and Quartic Nonlinearity
 - E. Central Part of $P(V, t)$
 - F. Discussion
 - VII. Summary
- Acknowledgements
- References
- VIII. Appendix. Numerical Solution Methods
 - A. Numerical Solution of the Fractional Fokker–Planck Equation [Eq. (38)] via the Grünwald–Letnikov Method
 - B. Numerical Solution of the Langevin Equation [Eq. (25)]

I. INTRODUCTION

Random processes in the physical and related sciences have a long-standing history. Beginning with the description of the haphazard motion of dust particles seen against the sunlight in a dark hallway in the astonishing work of Titus Lucretius Carus [1], followed by Jan Ingenhousz’s record of jittery motion of charcoal on an alcohol surface [2] and Robert Brown’s account of zigzag motion of pollen particles [3], made quantitative by Adolf Fick’s introduction of the diffusion equation as a model for spatial spreading of epidemic diseases [6], and culminating with Albert Einstein’s theoretical description [4] and Jean Perrin’s experiments tracing the motion of small particles of putty [5], the idea of an effective stochastic motion of a particle in a surrounding heat bath has been a triumph of the statistical approach to complex systems. This is even more true in the present Einstein year celebrating 100 years after his groundbreaking work providing our present understanding of Brownian motion. In Fig. 1, we display a collection of typical trajectories collected by Perrin.

Classical Brownian motion of a particle is distinguished by the linear growth of the mean-square displacement of its position coordinate x [9–11],¹

$$\langle x^2(t) \rangle \simeq Dt \tag{1}$$

¹*Editor’s note.* The inertia of the particle is ignored.

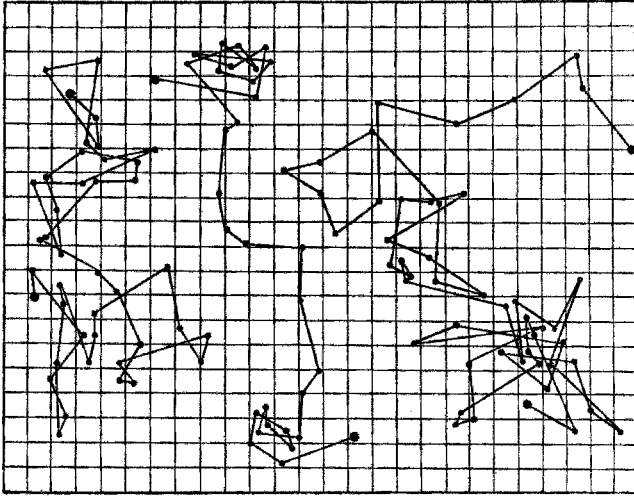


Figure 1. Random walk traces recorded by Perrin [5]: Three trajectories obtained by tracing a small grain of putty at intervals of 30sec. Using Einstein’s relation between the macroscopic gas constant and the diffusion constant, Perrin found a quite accurate result for Avogadro’s number. Refined results were successively obtained by Westgren and Kappler [7,8].

and the Gaussian form

$$P(x, t) = \frac{1}{\sqrt{4\pi Dt}} \exp\left(-\frac{x^2}{4Dt}\right) \tag{2}$$

of its probability density function (PDF) $P(x, t)$ to find the particle at position x at time t . This PDF satisfies the diffusion equation

$$\frac{\partial}{\partial t} P(x, t) = D \frac{\partial^2}{\partial x^2} P(x, t) \tag{3}$$

for natural boundary conditions $P(|x| \rightarrow \infty, t) = 0$ and δ function initial condition $P(x, 0) = \delta(x)$. If the particle moves in an external potential $V(x) = -\int^x F(x') dx'$, the force $F(x)$ it experiences enters additively into the diffusion equation, and the diffusion equation [Eq. (3)] is the particular term of the Fokker–Planck equation known as the Smoluchwski equation [11, 12]

$$\frac{\partial}{\partial t} P(x, t) = \left(\frac{\partial}{\partial x} \frac{V'(x)}{m\eta} + D \frac{\partial^2}{\partial x^2} \right) P(x, t) \tag{4}$$

where m is the mass of the particle and η the friction constant arising from existing from exchange of energy with the surrounding heat bath. This Fokker–Planck equation is a versatile instrument for the description of a stochastic process in external fields [12]. Requiring that the stationary solution defined by $\partial P(x, t)/\partial t = 0$ is the equilibrium distribution,

$$P_{\text{st}}(x) = \mathcal{N} \exp\left(-\frac{V'(x)}{Dm\eta}\right) \stackrel{!}{=} \mathcal{N} \exp\left(-\frac{V'(x)}{k_B T}\right) \quad (5)$$

where \mathcal{N} is the normalization constant and $k_B T$ the thermal energy, one obtains the Einstein–Stokes relation

$$D = \frac{k_B T}{m\eta} \quad (6)$$

for the diffusion constant. The second important relation connected with the Fokker–Planck equation [Eq. (4)] is the linear response

$$\langle x(t) \rangle_{F_0} = \frac{1}{2} F_0 \frac{\langle x^2(t) \rangle_{F=0}}{k_B T} \quad (7)$$

between the first moment (drift) in presence of a constant force F_0 and the variance in absence of that force, sometimes referred to as the second Einstein relation.

The Fokker–Planck equation can be obtained phenomenologically following Fick’s approach by combining the continuity equation with the constitutive equation for the probability current j ,

$$\frac{\partial}{\partial t} P(x, t) = -\frac{\partial}{\partial x} j(x, t), \quad j(x, t) = -D \frac{\partial}{\partial x} P(x, t) \quad (8)$$

Alternatively, that equation follows from the master equation [11]²

$$\frac{\partial}{\partial t} P(x, t) = \int \left\{ W(x|x') P(x', t) - W(x', x) P(x, t) \right\} dx' \quad (9)$$

by Taylor expansion of the transition probabilities W under specific conditions. The master equation is thus a balance equation for the “state” $P(x, t)$, and as such is a representation of a Pearson random walk: The transition probabilities quantify jumps from position x' to x and vice versa [11]. Finally, the Fokker–Planck equation emerges from the Langevin equation [13] (ignoring inertial effects)³:

$$\frac{dx(t)}{dt} = \frac{F(x)}{m\eta} + \Gamma(t) \quad (10)$$

²The differential form of the Chapman–Kolmogorov equation [11].

³That is, we consider the overdamped case.

relating the velocity of a particle to the external force, plus an erratic, time-fluctuating force $\Gamma(t)$. This random force $\Gamma(t)$ is supposed to represent the many small impacts on the particle by its surroundings (or heat bath); It constitutes a measure of our ignorance about the microscopic details of the “bath” to which the particle is coupled. On the typical scale of measurements, the Langevin description is, however, very successful. The random force $\Gamma(t)$ is assumed independent of x , and it fluctuates very rapidly in comparison to the variations of $x(t)$. We quantify this by writing

$$\overline{\Gamma(t)} = 0, \quad \overline{\Gamma(t)\Gamma(t')} = \Delta\delta(t - t') \tag{11}$$

where noise strength Δ and overbars denotes bath particle averages. δ denotes the Dirac-delta function, $\Gamma(t)$ is Gaussian, white noise which obeys Isserlis’s (Wick’s) theorem [13]. We will see below the differences which occur when the noise is no longer Gaussian.

Gaussian diffusion is by no means ubiquitous, despite the appeal of the central limit theorem. Indeed, many systems exhibit deviations from the linear time dependence of Eq. (1). Often, a nonlinear scaling of the form [14–16]

$$\langle x^2(t) \rangle \simeq Dt^\alpha \tag{12}$$

is observed, where the generalized diffusion coefficient now has the dimension $\text{cm}^2/\text{sec}^\alpha$. One distinguishes subdiffusion ($0 < \alpha < 1$) and sub-ballistic, enhanced diffusion ($1 < \alpha < 2$). Subdiffusive phenomena include charge carrier transport in amorphous semiconductors [17], tracer diffusion in catchments [18], or the motion of inclusions in the cytoskeleton [19], just to name a few.⁴ In general, subdiffusion corresponds to situations where the normal diffusion is slowed down by trapping events [21–25]. Conversely, sub-ballistic, enhanced diffusion can stem from advection among random directional motions [26,27], from trapping of a wave-like process [28], or in Knudsen diffusion [29,30,31], among others. Trapping processes in the language of continuous time random walk theory are characterized by a waiting time drawn from a waiting time distribution $\psi(t)$, exhibiting a long tail, $\psi(t) \simeq t^{-1-\beta}$, where $0 < \beta < 1$ [14,21,32]. Now no characteristic waiting time exists; and while this process endures longer and longer, waiting times may be drawn from this $\psi(t)$. The nonexistence of a characteristic waiting time alters the Markovian character of normal diffusion, giving rise to slowly decaying memory effects (‘semi-Markov’ character). Among other consequences, this causes the aging effects. From a probability theory point of view, such behavior corresponds to the limiting distribution of a sum of positive, independent identically distributed random

⁴An extensive overview can be found in Ref. [20].

variables with a diverging first moment, enforcing by the generalized central limit theorem a one-sided Lévy stable density with characteristic function [14,33,34]

$$\Psi(u) = \mathcal{L}\{\psi(t)\} \equiv \int_0^{\infty} e^{-ut} \psi(t) dt = e^{-(t/\tau)^\beta}, \quad 0 < \beta < 1. \quad (13)$$

The above relation is valid also for $\beta = 1$. Indeed, in that limit, we have $\psi(u) = e^{-t/\tau}$, whence $\psi(t) = \delta(t - \tau)$. This sharp distribution of the waiting time is but one possible definition of a Markovian process. In the remainder of this review, we solely focus on processes with $\beta = 1$.

Apart from trapping, there also exist situations where, as far as ensemble average $\langle \cdot \rangle$ is concerned, the mean square displacement does not exist. This corresponds to a jump length distribution $\lambda(x)$ emerging from an Lévy stable density for independent identically distributed random variables of the symmetric jump length x , whose second moment diverges. The characteristic function of this Lévy stable density is [14,33,34]

$$\lambda(k) = \mathcal{F}\{\lambda(x)\} \equiv \int_{-\infty}^{\infty} \lambda(x) e^{ikx} dx = \exp(-\sigma^\alpha |k|^\alpha) \quad (14)$$

for $0 < \alpha \leq 2$. For $\alpha = 2$, one immediately recovers a Gaussian jump length distribution with finite variance σ^2 . Figure 2 describes the data points for the

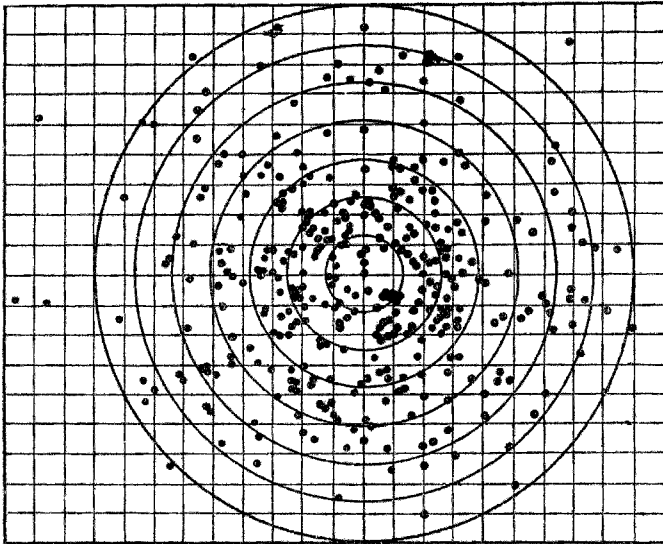


Figure 2. The starting point of each step from Fig. 1 is shifted to the origin. This illustrates the continuum approach of the jump length distribution if only a large number of jumps is considered [5].

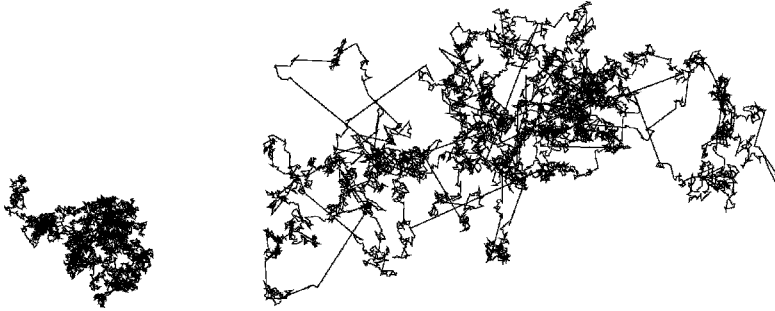


Figure 3. Comparison of the trajectories of a Gaussian (*left*) and a Lévy (*right*) process, the latter with index $\alpha = 1.5$. While both trajectories are statistically self-similar, the Lévy walk trajectory possesses a fractal dimension, characterizing the island structure of clusters of smaller steps, connected by a long step. Both walks are drawn for the same number of steps (~ 7000).

jump lengths collected by Perrin, which were then fitted to a Gaussian. Asymptotically for $0 < \alpha < 2$, relation (14) implies the long-tailed form

$$\lambda(x) \simeq |x|^{-1-\alpha} \tag{15}$$

During the random walk governed by $\lambda(x)$ with $0 < \alpha < 2$, longer and longer jump lengths occur, leading to a characteristic trajectory with fractal dimension α . Thus, processes with an underlying Lévy stable jump length distribution are called Lévy flights [35,36]. A comparison between the trajectory of a Gaussian and a Lévy flight process is shown in Fig. 3, for the same number of steps. A distinct feature of the Lévy flight is the hierarchical clustering of the trajectory. Lévy-flight processes have been assigned to spreading of biological species [37–39], related to the high efficiency of a Lévy flight as a search mechanism for exactly this exchange of long jumps and local exploration [40], in contrast to the locally oversampling (in one or two dimensions) of a Gaussian process. A number of trajectories monitored for the motion of spider monkeys are displayed in Fig. 4, along with the power-law motion length distribution for individual monkeys and the entire group [41]. Lévy flights have been also used to model groundwater flow [42], which exhibits Lévy stable features, these are implicated in plasma processes [43] and other turbulent phenomena, among many others, see, for instance [16,20]. It is worthwhile noting that a diverging kinetic energy has been reported for an ion in an optical lattice [44].

Lévy flights are the central topic of this review. For a homogeneous environment the central relation of continuous time random walk theory is given by [14,45]

$$P(k, u) = \frac{1 - \psi(u)}{u} \frac{1}{1 - \psi(u)\lambda(k)} \tag{16}$$

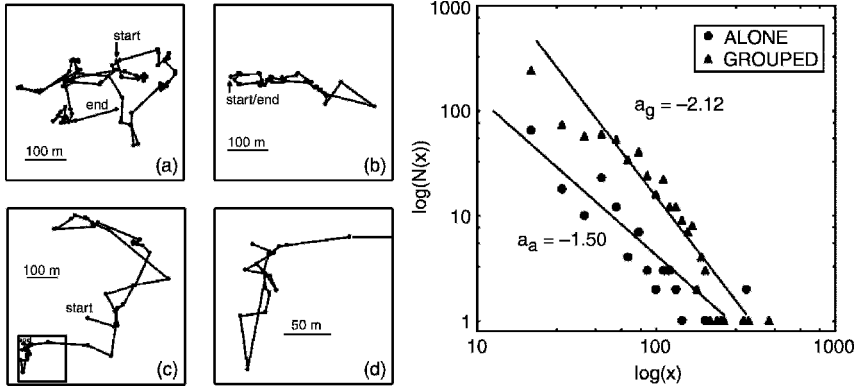


Figure 4. Daily trajectories of adult female (a,b) and male (c) spider monkeys. In panel d, a zoom into the square of c is shown [41]. On the right, the step length distribution is demonstrated to approximately follow power-law statistics with exponent a_g corresponding to Lévy motion.

that is, the Fourier–Laplace transform of the propagator, which immediately produces in the limit $k\sigma \rightarrow 0$ and $u\tau \rightarrow 0$ (i.e., long distance and long time limit, in comparison to σ and τ) the characteristic function

$$P(k, t) = \exp \left(-D|k|^\alpha t \right) \tag{17}$$

with diffusion coefficient $D = \sigma^\alpha/\tau$ with dimensions $\text{cm}^\alpha/\text{sec}$. That is, the PDF $P(x, t)$ of such a Lévy flight process is a Lévy stable density. In particular, it decays like $P(x, t) \simeq Dt/|x|^{1+\alpha}$. Although the variance of Lévy flights diverges, one can obtain by means of rescaling of fractional moments a relation that is formally equivalent to expression (1), namely [46]

$$\langle |x|^\zeta \rangle^{2/\zeta} \simeq Dt^{2/\alpha} \tag{18}$$

where $0 < \zeta < \alpha$ for convergence. This scaling relation indicates that Lévy flights are indeed move superdiffusively. We note here that instead of the decoupled jump length and waiting time distributions used in this continuous time random walk description of Lévy flights, one can introduce a coupling between $\lambda(x)$ and $\psi(t)$, such that long jumps invoke a higher time cost than short jumps. Such a coupling therefore introduces a finite “velocity,” leading to the name Lévy walks, compare [45,47,48]. These are non-Markovian processes, which we shall not consider any further.

Continuous time random walk processes with decoupled $\lambda(x)$ and $\psi(t)$ can be rephrased in terms of a generalized master equation [49]. This is also true for a general external force $F(x)$, where we obtain a relation of the type

$$\frac{\partial}{\partial t}P(x, t) = \int_{-\infty}^{\infty} dx' \int_0^t dt' \mathfrak{K}(x, x', t - t')P(x', t') \tag{19}$$

The kernel \mathfrak{K} determines the jump length dependence of the starting position x' , as well as the waiting time. Only in the spatially homogeneous case, is $\mathfrak{K}(x, x', t - t') = \mathfrak{K}(x - x', t - t')$ [50,51]. In continuous time random walk language, one needs to replace $\lambda(x)$ by $\Lambda(x, x')$ [52].

A convenient way to formulate a dynamical equation for a Lévy flight in an external potential is the space-fractional Fokker–Planck equation. Let us quickly review how this is established from the continuous time random walk. We will see below, how that equation also emerges from the alternative Langevin picture with Lévy stable noise. Consider a homogeneous diffusion process, obeying relation (16). In the limit $k \rightarrow 0$ and $u \rightarrow 0$, we have $\lambda(k) \sim 1 - \sigma^\alpha |k|^\alpha$ and $\psi(u) \sim 1 - u\tau$, whence [52–55]

$$uP(k, u) - 1 = -D|k|^\alpha P(k, u) \tag{20}$$

From the differentiation theorem of Laplace transform, $\mathcal{L}\{\dot{f}(t)\} = uP(u) - P(t = 0)$, we infer that the left-hand side in (x, t) space corresponds to $\partial P(x, t)/\partial t$, with initial condition $P(x, 0) = \delta(x)$. Similarly in the Gaussian limit $\alpha = 2$, the right-hand side is $D\partial^2 P(x, t)/\partial x^2$, so that we recover the standard diffusion equation. For general α , the right-hand side defines a fractional differential operator in the Riesz–Weyl sense (see below) and we find the fractional diffusion equation [52–56]

$$\frac{\partial}{\partial t}P(x, t) = D \frac{\partial^\alpha}{\partial |x|^\alpha} P(x, t) \tag{21}$$

where we interpret $\mathcal{F}\{\partial^\alpha g(x)/\partial |x|^\alpha\} = -|k|^\alpha g(k)$. The drift exerted by the external force $F(x)$ should enter additively (as proved in Ref. 52), and we finally obtain the fractional Fokker–Planck equation for Lévy flight processes, [52,54–56]

$$\frac{\partial}{\partial t}P(x, t) = \left(\frac{\partial}{\partial x} \frac{V'(x)}{m\eta} + D \frac{\partial^\alpha}{\partial |x|^\alpha} \right) P(x, t) \tag{22}$$

The fractional Fokker–Planck equation (22) which ignores inertial effects can be solved exactly for an harmonic potential (Ornstein–Uhlenbeck process),

giving rise to the restoring Hookean force $F(x) = -m\omega^2x$. In the space of wavenumbers k , the solution is [57]

$$P(k, t) = \exp\left(-\frac{\eta D |k|^\alpha}{\alpha \omega^2} \left[1 - e^{-\alpha \omega^2 t / \eta}\right]\right) \quad (23)$$

which is a Lévy stable density with the same stable index α , but time-dependent width $\eta D / (\alpha \omega) \times [1 - \exp(-\alpha \omega^2 t / \eta)]$. In particular, the stationary solution

$$P_{\text{st}}(x) = \mathcal{F}^{-1}\left\{\exp\left(-\frac{\eta D |k|^\alpha}{\alpha \omega^2}\right)\right\} \sim \frac{\eta D}{\alpha \omega^2 |x|^{1+\alpha}} \quad (24)$$

leads to an infinite variance. Thus, although the harmonic potential introduces a linear restoring force, the process never leaves the basin of attraction of the Lévy stable density with index α , imposed by the external noise. In particular, due to the diverging variance, the Einstein–Stokes relation and the linear response found for standard diffusion,⁵ no longer hold.

After addressing the Langevin and fractional Fokker–Planck formulations of Lévy flight processes in some more detail, we will show that in the presence of steeper than harmonic external potentials, the situation changes drastically: The forced Lévy process no longer leads to an Lévy stable density but instead to a *multimodal* PDF with *steeper asymptotics than any Lévy stable density*.

Multimodality of the PDF and a converging variance are just one result, which one would not expect at first glance. We will show that Lévy flights in the presence of non-natural boundary conditions are incompatible with the method of images, leading to subtleties in the first passage and first arrival behaviour. Moreover, we will demonstrate how a driving Lévy noise alters the standard Kramers barrier crossing problem, thereby preserving the exponential decay of the survival probability. Finally, we address the long-standing question of whether or not a Lévy flight with a diverging variance (or diverging kinetic energy) exhibits pathological behavior. As we will show, within a proper framework, nonlinear dissipative effects will cause a truncation of the Lévy stable nature; however, within a finite experimental window, Lévy flights are a meaningful approximation to real systems. These questions touch on the most fundamental properties of a stochastic process, and the question of the thermodynamic interpretation of processes that leave the basin of attraction of standard Gaussian processes. Lévy flights, despite having been studied for many decades, still leave numerous open questions. In the following we explore the new physics of Lévy flight processes and demonstrate their subtle and the intriguing nature.

⁵And, in generalized form, also for subdiffusive processes [58].

II. DEFINITION AND BASIC PROPERTIES OF LÉVY FLIGHTS

In this section, we formulate the dynamical description of Lévy flights using both a stochastic differential (Langevin) equation and the deterministic fractional Fokker–Planck equation. For the latter, we also discuss the corresponding form in the domain of wavenumbers, which is a convenient form for certain analytical manipulations in later sections.

A. The Langevin Equation with Lévy Noise

Our starting point in the stochastic description is the overdamped Langevin equation [54,59]⁶

$$\frac{dx}{dt} = \frac{F(x)}{m\eta} + \Gamma_\alpha(t) \tag{25}$$

where $F = -dV/dx$ is an external force with potential $V(x)$, which we choose to be

$$V(x) = \frac{a|x|^c}{c} \tag{26}$$

with amplitude $a > 0$ and exponent $c \geq 2$ (for reasons that become clear below); as before, m is the particle mass, η the friction coefficient, and $\Gamma_\alpha(t)$ represents a stationary white Lévy noise with Lévy index α ($1 \leq \alpha \leq 2$). By white Lévy noise $\Gamma_\alpha(t)$ we mean that the process

$$L(\Delta t) = \int_t^{t+\Delta t} \Gamma_\alpha(\tau) d\tau \tag{27}$$

that is, the time integral over an increment Δt , is an α -stable process with stationary independent increments. Restricting ourselves to symmetric Lévy stable distributions, this implies a characteristic function of the form

$$p_\alpha(k, \Delta t) = \exp(-D|k|^\alpha \Delta t) \tag{28}$$

The constant D in this description constitutes the intensity of the external noise.

In Fig. 5 we show realizations of white Lévy noises for various values of α . The sharply pronounced ‘spikes’, due to the long-tailed nature of the Lévy stable distribution, are distinctly apparent in comparison to the Gaussian case $\alpha = 2$.

⁶A more formal way of writing this Langevin equation is

$$x(t + dt) - x(t) = -\frac{1}{m\eta} \frac{dV(x)}{dx} dt + D^{1/\alpha} \Gamma_\alpha(dt)$$

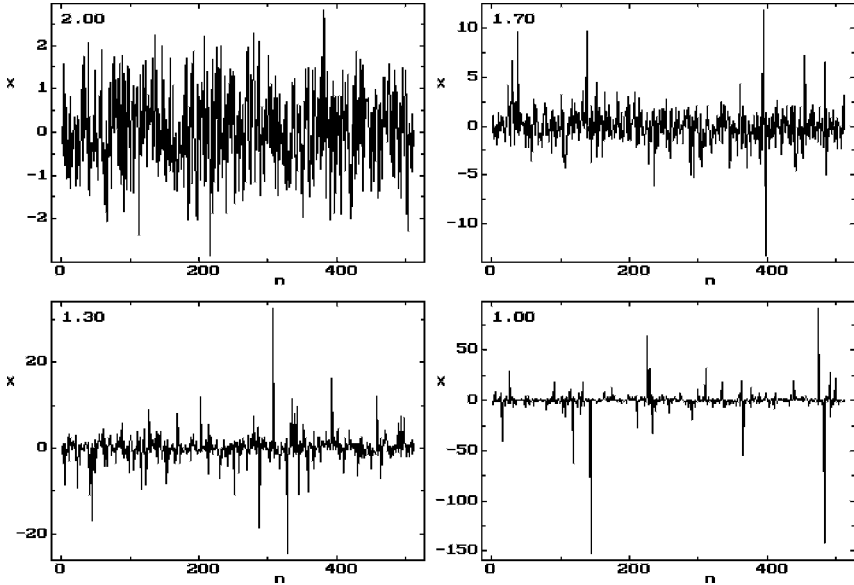


Figure 5. Examples of white Lévy noise with Lévy index $\alpha = 2, 1.7, 1.3, 1.0$. The outliers are increasingly more pronounced the smaller the Lévy index α becomes. Note the different scales on the ordinates.

B. Fractional Fokker–Planck Equation

The Langevin equation [Eq. (25)] still defines a Markov process, and it is therefore fairly straightforward to show that the corresponding fluctuation-averaged (deterministic) description is given in terms of the space-fractional Fokker–Planck equation (22) [54,60]. In what follows, we solve it with δ -initial condition

$$P(x, 0) = \delta(x) \tag{29}$$

The space-fractional derivative $\partial^\alpha / \partial |x|^\alpha$ occurring in the fractional Fokker–Planck equation (22) is called the Riesz fractional derivative. We have already seen that it is implicitly defined by

$$\mathcal{F} \left\{ \frac{\partial^\alpha P(x, t)}{\partial |x|^\alpha} \right\} = -|k|^\alpha P(k, t). \tag{30}$$

The Riesz fractional derivative is defined explicitly, via the Weyl fractional operator

$$\frac{d^\alpha P(x, t)}{d|x|^\alpha} = \begin{cases} -\frac{D_x^\alpha P(x, t) + D_x^\alpha P(x, t)}{2 \cos(\pi\alpha/2)}, & \alpha \neq 1 \\ -\frac{d}{dx} HP(x, t), & \alpha = 1 \end{cases} \tag{31}$$

where we use the following abbreviations:

$$(\mathbf{D}_+^\alpha P)(x, t) = \frac{1}{\Gamma(2 - \alpha)} \frac{d^2}{dx^2} \int_{-\infty}^x \frac{P(\xi, t) d\xi}{(x - \xi)^{\alpha-1}} \tag{32}$$

and

$$(\mathbf{D}_-^\alpha P)(x, t) = \frac{1}{\Gamma(2 - \alpha)} \frac{d^2}{dx^2} \int_x^\infty \frac{P(\xi, t) d\xi}{(\xi - x)^{\alpha-1}} \tag{33}$$

for the left and right Riemann–Liouville derivatives ($1 \leq \alpha < 2$), respectively, and [61]

$$(\mathbf{HP})(x, t) = \frac{1}{\pi} \int_{-\infty}^\infty \frac{P(\xi, t) d\xi}{x - \xi} \tag{34}$$

is the Hilbert transform. Note that the integral is to be interpreted as the Cauchy principal value. The definitions of $\partial^\alpha / \partial |x|^\alpha$ demonstrate the strongly nonlocal property of the space-fractional Fokker–Planck equation.

1. Rescaling of the Dynamical Equations

Passing to dimensionless variables

$$x' = x/x_0, \quad t' = t/t_0 \tag{35}$$

with

$$x_0 = \left(\frac{mD\eta}{a} \right)^{1/(c-2+\alpha)}, \quad t_0 = \frac{x_0^c}{D} \tag{36}$$

the initial equations take the form (we omit primes below)

$$\frac{dx}{dt} = -\frac{dV}{dx} + \Gamma_\alpha(t) \tag{37}$$

instead of the Langevin equation (25), and

$$\frac{\partial P(x, t)}{\partial t} = \frac{\partial}{\partial x} \frac{dV}{dx} P(x, t) + \frac{\partial^\alpha P(x, t)}{\partial |x|^\alpha} \tag{38}$$

instead of the fractional Fokker–Planck equation (22); also,

$$V(x) = \frac{|x|^c}{c} \tag{39}$$

instead of Eq. (26).

C. Starting Equations in Fourier Space

For the PDF $P(x, t)$ and its Fourier image $P(k, t) = \mathcal{F}\{P(x, t)\}$, we use the notation

$$P(x, t) \div P(k, t), \tag{40}$$

where the symbol \div denotes a Fourier transform pair. Since [62]

$$\mathbf{D}_\pm^\alpha P(x, t) \div (\mp ik)^\alpha P(k, t) \tag{41}$$

and

$$\mathbf{H}P(x, t) \div \text{isign}(k)P(k, t) \tag{42}$$

we obtain

$$\frac{\partial^\alpha P(x, t)}{\partial |x|^\alpha} \div -|k|^\alpha P(k, t) \tag{43}$$

for all α . The transformed fractional Fokker–Planck equation [Eq. (38)] for the characteristic function then follows immediately:

$$\frac{\partial P(k, t)}{\partial t} + |k|^\alpha P(k, t) = V_k P(k, t) \tag{44}$$

with the initial condition

$$P(k, t = 0) = 1 \tag{45}$$

and the normalization

$$P(k = 0, t) = 1 \tag{46}$$

The external potential $V(x)$ becomes the linear differential operator in k ,

$$\begin{aligned} V_k P(x, t) &= \int_{-\infty}^{\infty} e^{ikx} \frac{\partial}{\partial x} \left(\frac{dV}{dx} P(x, t) \right) dx \\ &= -ik \int_{-\infty}^{\infty} e^{ikx} \text{sign}(x) |x|^{c-1} P(x, t) dx \end{aligned} \tag{47}$$

Next, by using the following inverse transforms

$$(\pm ix)^\alpha P(x) \div \mathbf{D}_\pm^\alpha P(k) \tag{48}$$

and

$$-i(\text{sign}(x)P(x) \div \mathbf{H}P(k)) \quad (49)$$

we obtain the explicit expression for the external potential operator,

$$V_k P(k, t) = \begin{cases} \frac{k}{2\cos(\pi c/2)} (\mathbf{D}_+^{c-1} - \mathbf{D}_-^{c-1}) P(k, t), & c \neq 3, 5, 7, \dots \\ (-1)^m k \frac{d^{2m}}{dk^{2m}} \mathbf{H}P(k, t), & c = 3, 5, 7, \dots \end{cases} \quad (50)$$

Note that for the even potential exponents $c = 2m + 2$, $m = 0, 1, 2, \dots$, we find the simplified expression

$$V_k = (-1)^{m+1} k \frac{\partial^{2m+1}}{\partial k^{2m+1}} \quad (51)$$

in terms of conventional derivatives in k . We see that the force term can be written in terms of fractional derivatives in k -space, and therefore it is not straightforward to calculate even the stationary solution of the fractional Fokker–Planck equation [Eq. (38)] in the general case $c \notin \mathbb{N}$. In particular, in this latter case, the nonlocal equation [Eq. (38)] in x -space translates into a nonlocal equation in k -space, where the nonlocality shifts from the diffusion to the drift term.

III. CONFINEMENT AND MULTIMODALITY

In the preceding section, we discussed some elementary properties of the space-fractional Fokker–Planck equation for Lévy flights; in particular, we highlighted in the domain of wave numbers k the spatially nonlocal character of Eq. (38), and its counterpart (44). For the particular case of the external harmonic potential corresponding to Eq. (26) with $c = 2$, we found that the PDF does not leave the basin of attraction imposed by the external noise $\Gamma_\alpha(t)$ —that is, its stable index α . In this section, we determine the analytical solution of the fractional Fokker–Planck equation for general $c \geq 2$. We start with the exactly solvable stationary quartic Cauchy oscillator, to demonstrate directly the occurring *steep asymptotics* and the *bimodality*, that we will then investigate in the general case. The findings collected in this section were first reported in Refs. 60, 63 and 64.

A. The Stationary Quartic Cauchy Oscillator

Let us first consider a stationary quartic potential with $c = 4$ for the Cauchy–Lévy flight with $\alpha = 1$ that is, the solution of the equation

$$\frac{d}{dx} x^3 P_{\text{st}}(x) + \frac{d}{d|x|} P_{\text{st}}(x) = 0 \quad (52)$$

or

$$\frac{d^3 P_{\text{st}}(k)}{dk^3} = \text{sign}(k)|k|P_{\text{st}}(k) \quad (53)$$

in the k domain. Its solution is

$$P_{\text{st}}(k) = \frac{2}{\sqrt{3}} \exp\left(-\frac{|k|}{2}\right) \cos\left(\frac{\sqrt{3}|k|}{2} - \frac{\pi}{6}\right) \quad (54)$$

whose inverse Fourier transform results in the simple analytical form

$$P_{\text{st}}(x) = \frac{1}{\pi(1 - x^2 + x^4)}. \quad (55)$$

We observe surprisingly that the variance

$$\langle x^2 \rangle = 1 \quad (56)$$

of the solution (55) is *finite*, due to the long-tailed asymptotics $P_{\text{st}}(x) \sim x^{-4}$. In addition, as shown in Fig. 6, this solution has *two global maxima* at $x_{\text{max}} = \pm 1/\sqrt{2}$ along with the local minimum at the origin (that is the position of the initial condition). These two distinct properties of Lévy flights are a central theme of the remainder of this section.

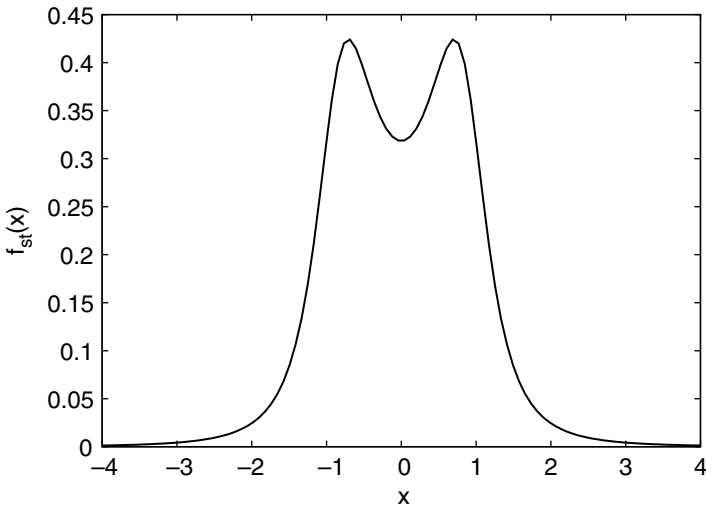


Figure 6. Stationary PDF (55) of the Cauchy-Lévy flight in a quartic ($c = 4$) potential. Two global maxima exist at $x_{\text{max}} = \pm 1/\sqrt{2}$, and a local minimum at the origin also exists.

B. Power-Law Asymptotics of Stationary Solutions for $c \geq 2$, and Finite Variance for $c > 2$

We now derive the power-law asymptotics of the stationary PDF $P_{\text{st}}(x)$ for external potentials of the form (39) with general $c \geq 2$. Thus, we note that as $x \rightarrow +\infty$, it is reasonable to assume

$$\mathbf{D}_-^\alpha P_{\text{st}} \ll \mathbf{D}_+^\alpha P_{\text{st}} \tag{57}$$

since the region of integration for the right-side Riemann–Liouville derivative $\mathbf{D}_-^\alpha P_{\text{st}}(x)$, (x, ∞) , is much smaller than the region of integration for the left-side derivative $\mathbf{D}_+^\alpha P_{\text{st}}(x)$, $(-\infty, x)$, in which the major portion of $P_{\text{st}}(x)$ is located. Thus, at large x we get for the stationary state,

$$\frac{d}{dx} \left(\frac{dV}{dx} P_{\text{st}}(x) \right) - \frac{1}{2 \cos(\pi\alpha/2)} \frac{d^2}{dx^2} \int_{-\infty}^x \frac{P_{\text{st}}(\xi) d\xi}{(x - \xi)^{\alpha-1}} \cong 0 \tag{58}$$

This relation corresponds to the approximate equality

$$x^{c-1} P_{\text{st}}(x) \cong \frac{1}{2 \cos(\pi\alpha/2)} \frac{d}{dx} \int_{-\infty}^x \frac{P_{\text{st}}(\xi) d\xi}{(x - \xi)^{\alpha-1}} \tag{59}$$

We are seeking asymptotic behaviors of $P_{\text{st}}(x)$ in the form $P(x) \approx C_1/x^\mu$ ($x \rightarrow +\infty$, $\mu > 0$). After integration of relation (59), we find

$$\frac{2C_1 \cos(\pi\alpha/2)\Gamma(2 - \alpha)}{-\mu + c} x^{-\mu+c} \cong \int_{-\infty}^x \frac{P_{\text{st}}(\xi) d\xi}{(x - \xi)^{\alpha-1}} \tag{60}$$

The integral on the right-hand side can be approximated by

$$\frac{1}{x^{\alpha-1}} \int_{-\infty}^x P_{\text{st}}(\xi) d\xi \cong \frac{1}{x^{\alpha-1}} \int_{-\infty}^{\infty} P_{\text{st}}(\xi) d\xi = \frac{1}{x^{\alpha-1}} \tag{61}$$

Thus, we may identify the powers of x and the prefactor, so that

$$\mu = \alpha + c - 1 \tag{62}$$

and

$$C_1 = \frac{\sin(\pi\alpha/2)\Gamma(\alpha)}{\pi} \tag{63}$$

By symmetry of the PDF we therefore recover the general asymptotic form

$$P_{\text{st}}(x) \approx \frac{\sin(\pi\alpha/2)\Gamma(\alpha)}{\pi|x|^\mu}, \quad x \rightarrow +\infty \quad (64)$$

for all $c \geq 2$. This result is remarkable, for several reasons:

- (i) despite the approximations involved, the asymptotic form (64) for arbitrary $c \geq 2$ corresponds exactly to previously obtained forms, such as the exact analytical result for the harmonic Lévy flight (linear Lévy oscillator), $c = 2$ reported in Ref. 57; the result for the quartic Lévy oscillator with $c = 4$ discussed in Ref. 60 and 64; and the case of even power-law exponents $c = 2m + 2$ ($m \in \mathbb{N}_0$) given in Ref. 60. It is also supported by the calculation in Ref. 65.
- (ii) The prefactor C_1 is independent of the potential exponent c ; in this sense, C_1 is universal.
- (iii) For each value α of the Lévy index a critical value

$$c_{\text{cr}} = 4 - \alpha \quad (65)$$

exists such that at $c < c_{\text{cr}}$ the variance $\langle x^2 \rangle$ is infinite, whereas at $c > c_{\text{cr}}$ the variance is *finite*.

- (iv) We have found a fairly simple method for constructing stationary solutions for large x in the form of inverse power series.

The qualitative consequence of the steep power-law asymptotics can be visualized by direct integration of the Langevin equation for white Lévy noise, the latter being portrayed in Fig. 5. Typical results for the sample paths under the influence of an external potential (39) with increasing superharmonicity are shown in Fig. 7 in comparison to the Brownian case (i.e., white Gaussian noise). For growing exponent c , the long excursions typical of homogeneous Lévy flights are increasingly suppressed. For all cases shown, however, the qualitative behavior of the noise under the influence of the external potential is different from the Brownian noise even in this case of strong confinement. In the same figure, we also show the curvature of the external potential. Additional investigations have shown that the maximum curvature is always very close to the positions of the two maxima, leading us to conjecture that they are in fact identical.

C. Proof of Nonunimodality of Stationary Solution for $c > 2$

In this subsection we demonstrate that the stationary solution of the kinetic equation (38) has a nonunimodal shape. For this purpose, we use an

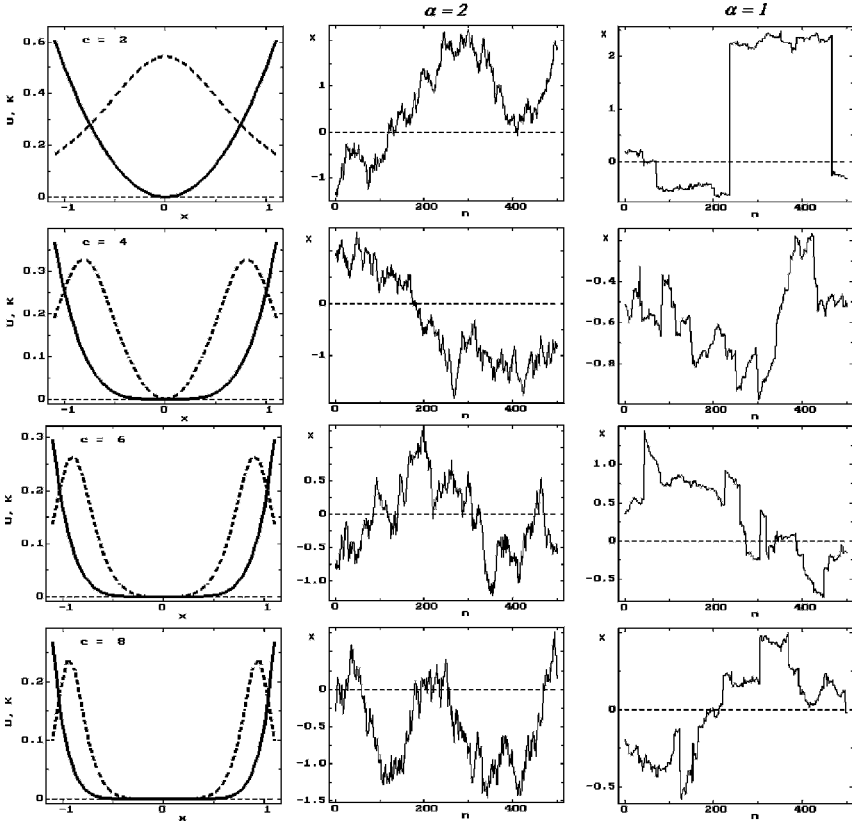


Figure 7. *Left column:* The potential energy functions $V = x^c/c$, (solid lines) and their curvatures (dotted lines) for different values of c : $c = 2$ (linear oscillator), and $c = 4, 6, 8$ (strongly non-linear oscillators). *Middle column:* Typical sample paths of Brownian oscillators, $\alpha = 2$, with the potential energy functions shown on the left. *Right column:* Typical sample paths of Lévy oscillators, $\alpha = 1$. On increasing m the potential walls become steeper, and the flights become shorter; in this sense, they are confined.

alternative expression for the fractional Riesz derivative (compare, e.g., Ref. 62),

$$\frac{d^\alpha P(x)}{d|x|^\alpha} \equiv \Gamma(1 + \alpha) \frac{\sin(\alpha\pi/2)}{\pi} \times \int_0^\infty d\xi \frac{P(x + \xi) - 2P(x) + P(x - \xi)}{\xi^{1+\alpha}} \quad (66)$$

valid for $0 < \alpha < 2$. In the stationary state ($\partial P / \partial t = 0$), we have from Eq. (38)

$$\frac{d}{dx} \left(\text{sgn}(x) |x|^{c-1} P_{\text{st}}(x) \right) + \frac{d^2 P_{\text{st}}(x)}{d|x|^\alpha} = 0 \tag{67}$$

Thus, it follows that at $c > 2$ (strict inequality)

$$\left. \frac{d^2 P_{\text{st}}(x)}{d|x|^\alpha} \right|_{x=0} = 0 \tag{68}$$

or, from definition (66) and noting that $P_{\text{st}}(x)$ is an even function,

$$\int_0^\infty d\xi \frac{P_{\text{st}}(\xi) - P_{\text{st}}(0)}{\xi^{1+\alpha}} = 0 \tag{69}$$

we can immediately obtain a proof of the nonunimodality of P_{st} , from the latter relation, which we produce in two steps:

1. If we assume that the stationary PDF $P_{\text{st}}(x)$ is unimodal, then due to the symmetry $x \rightarrow -x$, it necessarily has one global maximum at $x = 0$. Here the integrand in equation (69) must be negative, and therefore contradicts equation (69). Therefore, $P_{\text{st}}(x)$ is nonunimodal.
2. We can in addition exclude $P(0) = 0$, as now the integrand will be positive, which again contradicts Eq. (69).

Since $P(x) \rightarrow 0$ at $x \rightarrow \infty$, based on statements 1 and 2, one may conclude that the simplest situation is such that $\xi_0 > 0$ exists with the property

$$\int_{\xi_0}^\infty d\xi \frac{P(\xi) - P(0)}{\xi^{1+\alpha}} < 0 \tag{70}$$

and

$$\int_0^{\xi_0} d\xi \frac{P(\xi) - P(0)}{\xi^{1+\alpha}} > 0 \tag{71}$$

that is, the condition for a two-hump stationary PDF for all $c > 2$. At intermediate times, however, we will show that a trimodal state may also exist.

If such bimodality occurs, it results from a bifurcation at a critical time t_{12} [64] when evolution commences (as usually assumed) from the delta function at the origin. A typical result is shown in Fig. 8, for the quartic case $c = 4$ and

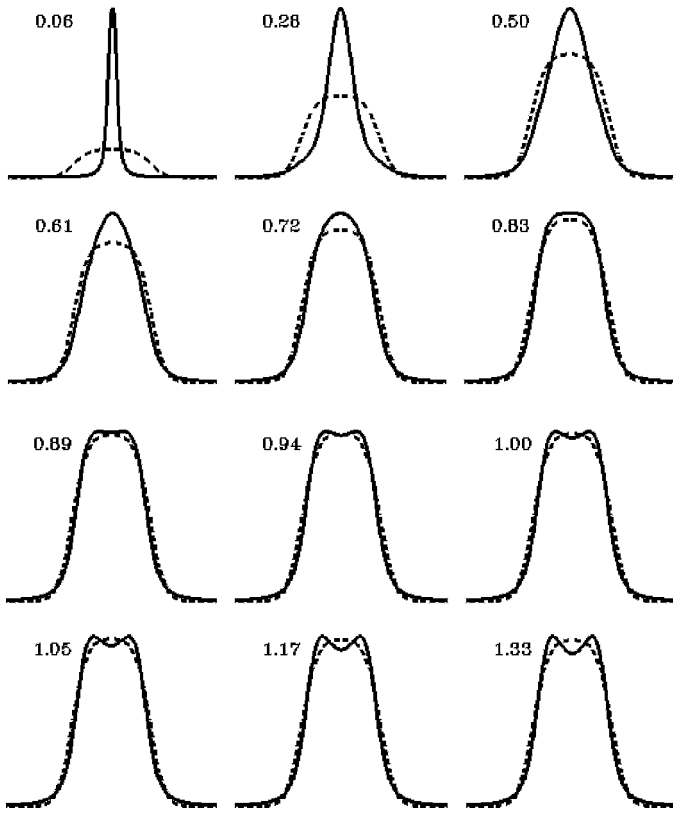


Figure 8. Time evolution of the Lévy flight-PDF in the presence of the superharmonic external potential [Eq. (26)] with $c = 4$ (quartic Lévy oscillator) and Lévy index $\alpha = 1.2$, obtained from the numerical solution of the fractional Fokker–Planck equation, using the Grünwald–Letnikov representation of the fractional Riesz derivative (full line). The initial condition is a δ -function at the origin. The dashed lines indicate the corresponding Boltzmann distribution. The transition from one to two maxima is clearly seen. This picture of the time evolution is typical for $2 < c \leq 4$ (see below).

Lévy index $\alpha = 1.2$: from an initial δ -peak, eventually a bimodal distribution emerges.

D. Formal Solution of Equation (38)

Returning to the general case, we rewrite Eq. (44) in the equivalent integral form,

$$P(k, t) = p_\alpha(k, t) + \int_0^t d\tau p_\alpha(k, t - \tau) V_k P(k, \tau) \tag{72}$$

where

$$p_\alpha(k, t) = \exp(-|k|^\alpha t) \quad (73)$$

is the characteristic function of a free (homogeneous) Lévy flight. This relation follows from equation (44) by formally treating it as a nonhomogeneous linear first-order differential equation, where V_k plays the role of the nonhomogeneity. Then, Eq. (44) is obtained by variation of parameters. [Differentiate Eq. (72) to return to Eq. (44).]

Equation (72) can be solved formally by iteration: Let

$$f^{(0)}(k, t) = p_\alpha(k, t) \quad (74)$$

then

$$f^{(1)}(k, t) = p_\alpha(k, t) + \int_0^t d\tau p_\alpha(k, t - \tau) V_k f^{(0)}(k, \tau) \quad (75)$$

$$f^{(2)}(k, t) = p_\alpha(k, t) + \int_0^t d\tau p_\alpha(k, t - \tau) V_k p_\alpha(k, \tau) + \int_0^t d\tau \int_0^\tau d\tau' p_\alpha(k, t - \tau) V_k p_\alpha(k, \tau - \tau') V_k p_\alpha(k, \tau') \quad (76)$$

and so on. From the convolution,

$$A * B = \int_0^t d\tau A(t - \tau) B(\tau) = \int_0^t d\tau A(\tau) B(t - \tau) \quad (77)$$

using

$$A * B * C = (A * B) * C = A * (B * C) \quad (78)$$

we arrive at the formal solution

$$P(k, t) = \sum_{n=0}^{\infty} p_\alpha(*V_k p_\alpha)^n \quad (79)$$

This procedure is analogous to perturbation theory, with $V_k P$ playing the role of the interaction term (see, for instance, Ref. 66, Chapter 16).

Applying a Laplace Transformation, namely,

$$P(k, u) = \int_0^{\infty} dt \exp(-ut) P(k, t) \quad (80)$$

to Eq. (72), we obtain

$$P(k, u) = p_\alpha(k, u) + p_\alpha(k, u)V_k P(k, u) \tag{81}$$

where

$$p_\alpha(k, u) = \frac{1}{u + k^\alpha} \tag{82}$$

is the Fourier–Laplace transform of the homogeneous Lévy stable PDF. Thus, we obtain the equivalent of the solution (79) in (k, u) -space:

$$P(k, u) = \sum_{n=0}^{\infty} [p_\alpha(k, u)V_k]^n p_\alpha(k, u) \tag{83}$$

This iterative construction scheme for the solution of the fractional Fokker–Planck equation will be useful below.

E. Existence of a Bifurcation Time

For the unimodal initial condition $P(x, 0) = \delta(x)$ we now prove the existence of a finite bifurcation time t_{12} for the turnover from a unimodal to a bimodal PDF. At this time, the curvature at the origin will vanish; that is, it is a point of inflection:

$$\left. \frac{\partial^2 P(x)}{\partial x^2} \right|_{x=0, t=t_{12}} = 0 \tag{84}$$

Introducing

$$J(t) = \int_0^{\infty} dk k^2 P(k, t) \tag{85}$$

Eq. (84) is equivalent to (note that the characteristic function is an even function)

$$J(t_{12}) = 0 \tag{86}$$

The bifurcation can now be obtained from the iterative solution (83); we consider the specific case $c = 4$. From the first-order approximation

$$P_1(k, u) = \frac{1}{u + k^\alpha} \left(1 + V_k \frac{1}{u + k^\alpha} \right) \tag{87}$$

where

$$V_k = k \frac{\partial^3}{\partial k^3} \tag{88}$$

Combining these two expressions, we have

$$P_1(k, u) = \frac{1}{u + k^\alpha} + \alpha(\alpha - 1)(2 - \alpha) \frac{k^{\alpha-2}}{(u + k^\alpha)^3} + 6\alpha^2(\alpha - 1) \frac{k^{2\alpha-2}}{(u + k^\alpha)^4} - 6\alpha^3 \frac{k^{3\alpha-2}}{(u + k^\alpha)^5} \quad (89)$$

or, on inverse Laplace transformation,

$$P_1(k, t) = e^{-k^\alpha t} \left\{ 1 - \frac{\alpha^3}{4} t^4 k^{3\alpha-2} + \alpha^2(\alpha - 1) t^3 k^{2\alpha-2} + \alpha(\alpha - 1)(2 - \alpha) \frac{t^2}{2} k^{\alpha-2} \right\} \quad (90)$$

The first approximation to the bifurcation time t_{12} is then determined via Eq. (85); that is, we calculate

$$\int_0^\infty dk k^2 P_1(k, t_{12}^{(1)}) = 0 \quad (91)$$

to obtain

$$t_{12}^{(1)} = \left(\frac{4\Gamma(3/\alpha)}{3(3 - \alpha)\Gamma(1/\alpha)} \right)^{\alpha/(2+\alpha)} \quad (92)$$

In Fig. 9, we show the dependence of this first approximation $t_{12}^{(1)}$ as a function of the Lévy index α (dashed line), in comparison to the values determined from the numerical solution of the fractional Fokker–Planck equation (38) shown as the dotted line. The second-order iteration for the PDF, $P_2(k, t)$, can be obtained with maple6, whence the second approximation for the bifurcation time is found by analogy with the above procedure. The result is displayed as the full line in Fig. 9. The two approximate results are in fact in surprisingly good agreement with the numerical result for the exact PDF. Note that the second approximation appears somewhat worse than the first; however, it contains the minimum in the α -dependence of the t_{12} behavior.

1. Trimodal Transient State at $c > 4$.

we have already proved the existence of a bimodal stationary state for the quartic ($c = 4$) Lévy oscillator. This bimodality emerges as a bifurcation at a critical time t_{12} , at which the curvature at the origin vanishes. This scenario is changed

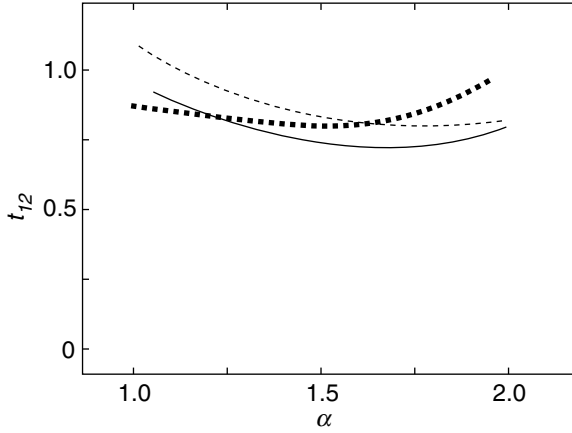


Figure 9. Bifurcation time t_{12} versus Lévy exponent α for external potential exponent $c = 4.0$. Black dots: bifurcation time deduced from the numerical solution of the fractional Fokker–Planck equation [Eq. (38)] using the Grünwald–Letnikov representation of the fractional Riesz derivative (see appendix). Dashed line: first approximation $t_{12}^{(1)}$; solid line: second approximation $t_{12}^{(2)}$.

for $c > 4$, as displayed in Fig. 10: There exists a transient trimodal form of the PDF. Thus, there are obviously two time scales that are relevant: the critical time for the emergence of the two off-center maxima, which are characteristic of the stationary state; and a second one, which corresponds to the relaxing initial central hump—that is, the decaying initial distribution $P(x, 0) = \delta(x)$. The formation of the two off-center humps while the central one is still present, as detailed in Fig. 11. The existence of a transient trimodal state was found to be typical for all $c > 4$.

2. Phase Diagrams for n -Modal States

The above findings can be set in the context of the purely bimodal case discussed earlier. A convenient way of displaying the n -modal character of the PDF in the presence of a superharmonic external potential of the type (39) is the phase diagram shown in Fig. 12. There, we summarize the findings that for $2 < c \leq 4$ the bifurcation occurs between the initial monomodal and the stationary bimodal PDF at a finite critical time, whereas for $c > 4$, a transient trimodal state exists. Moreover, we also include the shaded region, in which c is too small to ensure a finite variance. In Fig. 13, in complementary fashion the temporal domains of the n -modal states are graphed, and the solid lines separating these domains correspond to the critical time scales $t_{cr}(= t_{12}, t_{13}, t_{32})$. Again, the transient nature of the trimodal state is distinctly apparent.

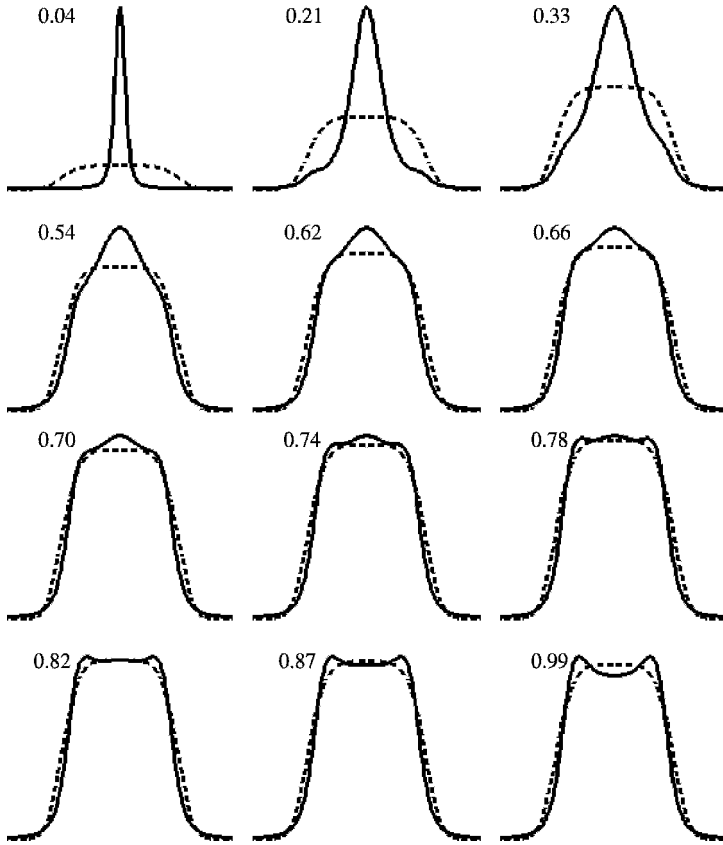


Figure 10. Time evolution of the PDF governed by the fractional Fokker–Planck equation (38) in a superharmonic potential (26) with exponent $c = 5.5$, and for Lévy index $\alpha = 1.2$, obtained from numerical solution using the Grünwald–Letnikov method explained in the appendix. Initial condition is $P(x, 0) = \delta(x)$. The dashed lines indicate the corresponding Boltzmann distribution. The transitions between $1 \rightarrow 3 \rightarrow 2$ humps are clearly seen. This picture of time evolution is typical for $c > 4$. On a finer scale, we depict the transient trimodal state in Fig. 11.

F. Consequences

By combining analytical and numerical results, we have discussed Lévy flights in a superharmonic external potential of power c . Depending on the magnitude of this exponent c , different regimes could be demonstrated. Thus, for $c = 2$, the character of the Lévy noise imprinted on the process, is not altered by the external potential: The resulting PDF has Lévy index α , the same as the noise itself, and will thus give rise to a diverging variance at all times. Conversely, for $c > 2$, the variance becomes finite if only $c > c_{\text{cr}} = 4 - \alpha$. Because the PDF no

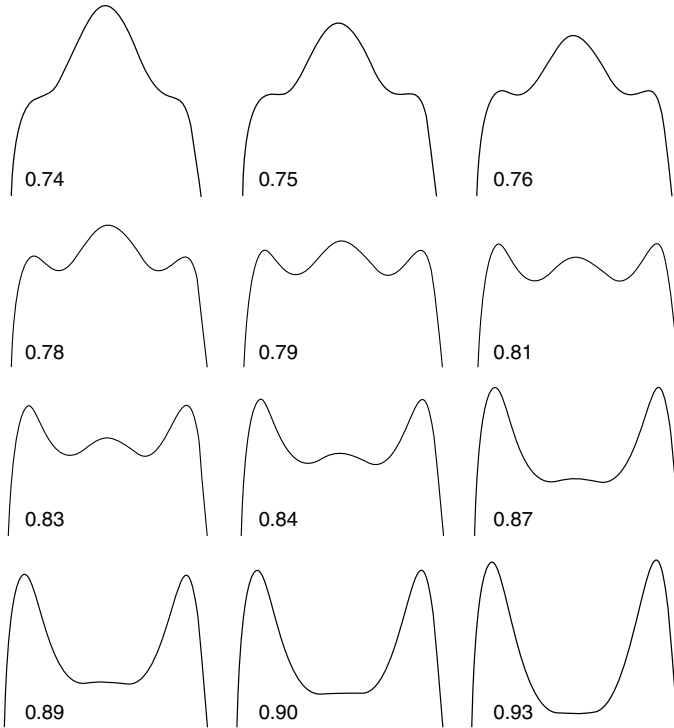


Figure 11. The transition $1 \rightarrow 3 \rightarrow 2$ from Fig. 10 on a finer scale ($c = 5.5, \alpha = 1.2$).

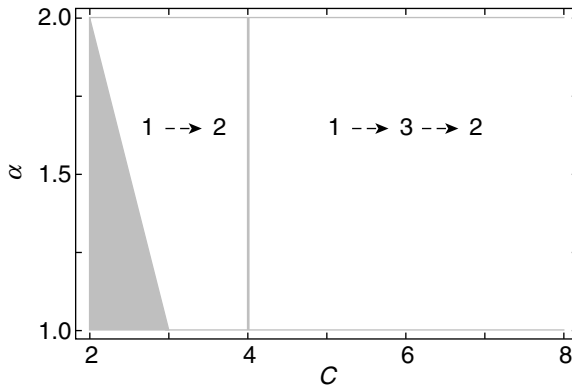


Figure 12. (c, α) map showing different regimes of the PDF. The region with infinite variance is shaded. The region $c < 4$ covers transitions from 1 to 2 humps during the time evolution. For $c > 4$, a transition from 1 to 3, and then from 3 to 2 humps occurs. In both cases, the stationary PDF exhibits 2 maxima. Compare Fig. 13.

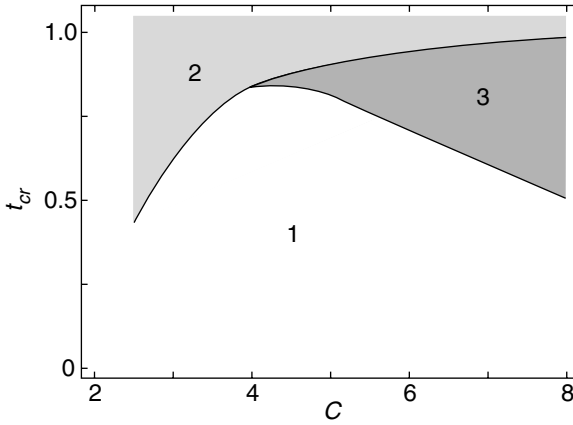


Figure 13. (c, t) map showing states of the PDF with different number of humps and the transitions between these. Region 1: The PDF has 1 hump. Region 2: The PDF exhibits 2 humps. Region 3: Three humps occur. At $c < 4$, there is only one transition $1 \rightarrow 2$, whereas for $c > 4$, there occur two transitions, $1 \rightarrow 3$ and $3 \rightarrow 2$.

longer belongs to the set of Lévy stable PDFs and acquires an inverse power-law asymptotic behavior with power $\mu = \alpha + c - 1$. Obviously, moments of higher order will still diverge. Apart from the finite variance, the PDF is distinguished by the observation that it bifurcates from the initial monomodal to a stationary bimodal state. If $c > 4$, there exists a transient trimodal state. This interesting behavior of the PDF both during relaxation and under stationary conditions, depending on a competition between Lévy noise and steepness of the potential is in contrast to the universal approach to the Boltzmann equilibrium, solely defined by the external potential, encountered in classical diffusion.

One may demand the exact kinetic reason for the occurrence of the multiple humps. Now the nontransient humps seem to coincide with the positions of maximum curvature of the external potential, which at these points changes almost abruptly for larger c from a rather flat to a very steep slope. Thus one may conclude that the random walker, which is driven towards these flanks by the anomalously strong Lévy diffusivity, is thwarted, thus the PDF accumulates close to these points. Apart from this rudimentary explanation, we do not yet have a more intuitive argument for the existence of the humps and their bifurcations, we also remark that other systems exist where multimodality occurs, for instance, in the transverse fluctuations of a grafted semiflexible polymer [67]. We will later return to the issue of finite variance in the discussion of the velocity distribution of a Lévy flight.

The different regimes for $c > 2$ can be classified in terms of critical quantities, in particular, the bifurcation time(s) $t_{\text{cr}} (= t_{12}, t_{13}, t_{32})$ and the critical

external potential exponent c_{cr} . Lévy flights in superharmonic potentials can then be conveniently represented by phase diagrams on the (c, α) and (c, t_{cr}) plains.

The numerical solution of both the fractional Fokker–Planck equation in terms of the Grünwald–Letnikov scheme used to find a discretized approximation to the fractional Riesz operator exhibits reliable convergence, as corroborated by direct solution of the corresponding Langevin equation.

Our findings have underlined the statement that the properties of Lévy flights, in particular under nontrivial boundary conditions or in an external potential are not fully understood. The general difficulty, which hampers a straightforward investigation as in the regular Gaussian or the subdiffusive cases, is connected with the strong spatial correlations associated with such problems, manifested in the integrodifferential nature of the Riesz fractional operator. Thus it is not easy to determine the stationary solution of the process. We expect, since diverging fluctuations appear to be relevant in physical systems, that many hitherto unknown properties of Lévy flights remain to be discovered. Some of these features are discussed in the following sections.

IV. FIRST PASSAGE AND ARRIVAL TIME PROBLEMS FOR LÉVY FLIGHTS

The first passage time density (FPTD) is of particular interest in random processes [14,68–70]. For Lévy flights, the first passage time density was determined by the method of images in a finite domain in reference [71], and by similar methods in reference [72]. These methods lead to results for the first passage time density in the semi-infinite domain, whose long-time behavior explicitly depends on the Lévy index α . In contrast, a theorem due to Sparre Andersen proves that for any discrete-time random walk process starting at $x_0 \neq 0$ with each step chosen from a continuous, symmetric but otherwise arbitrary distribution, the first passage time density asymptotically decays as $\sim n^{-3/2}$ with the number n of steps [70,73,74], being *fully independent* of the index of the Lévy flight—that is, universal. In the case of a Markov process, the continuous time analogue of the Sparre Andersen result reads [69,70]

$$p(t) \sim t^{-3/2} \quad (93)$$

The analogous universality was proved by Frisch and Frisch for the special case in which an absorbing boundary is placed at the source of the Lévy flight at $t > 0$ [75], and numerically corroborated by Zumofen and Klafter [76]. In the following, we demonstrate that the method of images is generally inconsistent with the universality of the first passage time density, and therefore cannot be applied to solve first passage time density-problems for Lévy flights. We also

show that for Lévy flights the first passage time density differs from the PDF for first arrival. The discussion will be restricted to the case $1 < \alpha < 2$ [77].

A. First Arrival Time

By incorporating in the fractional diffusion equation (21) a δ -sink of strength $p_{\text{fa}}(t)$, we obtain the diffusion-reaction equation for the non-normalized density function $f(x, t)$,

$$\frac{\partial}{\partial t} f(x, t) = D \frac{\partial^\alpha}{\partial |x|^\alpha} f(x, t) - p_{\text{fa}}(t) \delta(x) \quad (94)$$

from which by integration over all space, we may define the quantity

$$p_{\text{fa}}(t) = -\frac{d}{dt} \int_{-\infty}^{\infty} f(x, t) dx \quad (95)$$

that is, $p_{\text{fa}}(t)$ is the negative time derivative of the survival probability. By definition of the sink term, $p_{\text{fa}}(t)$ is the PDF of *first arrival*: once a random walker arrives at the sink, it is annihilated. By solving equation (94) by standard methods (determining the homogeneous and inhomogeneous solutions), it is straightforward to calculate the solution f in terms of the propagator P of the fractional diffusion equation (21) with initial condition $P(x, 0) = \delta(x - x_0)$ yielding $f(x, t) = [e^{ikx_0} + p(u)] / (u + D|k|^\alpha)$, whence $p_{\text{fa}}(t)$ satisfies the chain rule (p_{fa} implicitly depending on x_0)

$$P(-x_0, t) = \int_0^t p_{\text{fa}}(\tau) P(0, t - \tau) d\tau \quad (96)$$

which corresponds to the μ domain relation $p_{\text{fa}}(u) = P(-x_0, u) / P(0, u)$. Equation (96) is well known and for any sufficiently well-behaved continuum diffusion process is commonly used as a definition of the first passage time density [14,70].

For Gaussian processes with propagator $P(x, t) = 1/\sqrt{4\pi Dt} \exp(-x^2/[4Dt])$, one obtains by direct integration of the diffusion equation with appropriate boundary condition the first passage time density [70]

$$p(t) = \frac{x_0}{\sqrt{4\pi Dt^3}} \exp\left(-\frac{x_0^2}{4Dt}\right) \quad (97)$$

including the asymptotic behaviour $p(t) \sim t^{-3/2}$ for $t \gg x_0^2/(4D)$. In this Gaussian case, the quantity $p_{\text{fa}}(t)$ is equivalent to the first passage time density. From a random walk perspective, this occurs because individual steps all have the same increment, and the jump length statistics therefore ensure that the

walker cannot hop across the sink in a long jump without actually hitting the sink and being absorbed. The behaviour is very different for Lévy jump length statistics: There, the particle can easily cross the sink in a long jump. Thus, before eventually being absorbed, it can pass by the sink location many times, and therefore the statistics of the first arrival will be different from those of the first passage. In fact, with $P(x, u) = (2\pi)^{-1} \int_{-\infty}^{\infty} e^{ikx} (u + D|k|^\alpha)^{-1} dk$, we find

$$p_{fa}(u) = 1 - \frac{\int_0^\infty (1 - \cos kx_0)/(u + Dk^\alpha) dk}{\int_0^\infty 1/(u + Dk^\alpha) dk} \tag{98}$$

Since $\int_0^\infty (u + Dk^\alpha)^{-1} dk = \pi u^{1/\alpha-1}/(\alpha D^{1/\alpha} \sin(\pi/\alpha))$ and

$$\int_0^\infty \frac{1 - \cos kx_0}{u + Dk^\alpha} \sim \frac{\Gamma((2 - \alpha) \sin(\pi(2 - \alpha)/2)) x_0^{\alpha-1}}{(\alpha - 1)D}, \quad \text{for } u \rightarrow 0, \alpha > 1$$

we obtain the limiting form

$$p_{fa}(u) \sim 1 - x_0^{\alpha-1} u^{1-1/\alpha} D^{-1+1/\alpha} \tilde{\Lambda}(\alpha) \tag{99}$$

where $\tilde{\Lambda}(\alpha) = \alpha\Gamma(2 - \alpha) \sin(\pi(2 - \alpha)/2) \sin(\pi/\alpha)/(\alpha - 1)$. We note that the same result may be obtained using the exact expressions for $P(x_0, u)$ and $P(0, u)$ in terms of Fox H -functions and their series expansions [78]. The inverse Laplace transform of the small u -behavior (99) can be obtained by completing (99) to an exponential, and then computing the Laplace inversion using the identity $e^z = H_{0,1}^{1,0}[z|(0, 1)]$ in terms of the Fox H -function [78], for which the exact Laplace inversion can be performed [79]. Finally, series expansion of this result leads to the long- t form

$$p_{fa}(t) \sim C(\alpha) \frac{x_0^{\alpha-1}}{D^{1-1/\alpha} t^{2-1/\alpha}} \tag{100}$$

with $C(\alpha) = \alpha\Gamma(2 - \alpha)\Gamma(2 - 1/\alpha) \sin(\pi[2 - \alpha]/2) \sin^2(\pi/\alpha)/(\pi^2(\alpha - 1))$. Clearly, in the Gaussian limit, the required asymptotic form $p(t) \sim x_0/\sqrt{4\pi Dt^3}$ for the first passage time density is consistently recovered, whereas in the general case the result (100) is slower than in the universal first passage time density behavior embodied in Eq. (93), as it should be since the δ -trap used in equation (94) to define the first arrival for Lévy flights is weaker than the absorbing wall used to properly define the first passage time density. For Lévy flights, the PDF for first arrival thus scales like (100) (i.e., it explicitly depends on the index α of the underlying Lévy process), and, as shown below, it *differs* from the corresponding first passage time density.

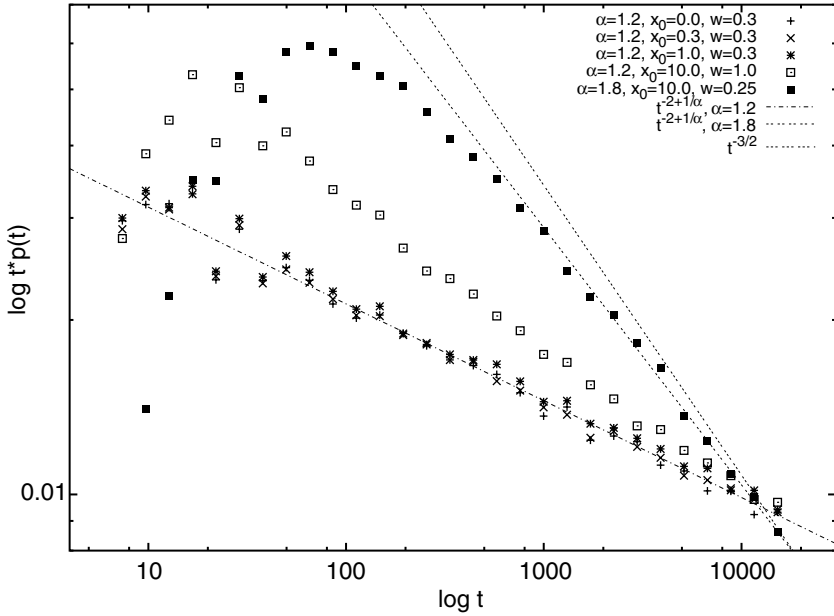


Figure 14. First arrival PDF for $\alpha = 1.2$ demonstrating the $t^{-2+1/\alpha}$ scaling, for optimal trap width $w = 0.3$. For comparison, we show the same scaling for $\alpha = 1.8$, and the power-law $t^{-3/2}$ corresponding to the first passage time density. The behavior for large $w = 1.0$ shows a shift of the decay toward the $-3/2$ slope. Note that the ordinate is $\lg tp(t)$. Note also that for the initial condition $x_0 = 0.0$, the trap is activated *after* the first step, consistent with Ref. [76].

Before calculating this first passage time density, we first demonstrate the validity of Eq. (100) by means of a simulation the results of which are shown in Fig. 14. Random jumps with Lévy flight jump length statistics are performed, and a particle is removed when it enters a certain interval of width w around the sink; in our simulations we found an optimum value $w \approx 0.3$. As seen in Fig. 14 (note that we plot $\lg tp(t)$!) and for analogous results not shown here, relation (100) is satisfied for $1 < \alpha < 2$, whereas for larger w , the slope increases.

B. Sparre Anderson Universality

To corroborate the validity of the Sparre Anderson universality, we simulate a Lévy flight in the presence of an absorbing wall—that is, random jumps with Lévy flight jump length statistics exist along the right semi-axis—and a particle is removed when it jumps across the origin to the left semi-axis. The results of such a detailed random walk study are displayed in Figs. 15 and 16. The expected universal $t^{-3/2}$ scaling is confirmed for various initial positions x_0 and

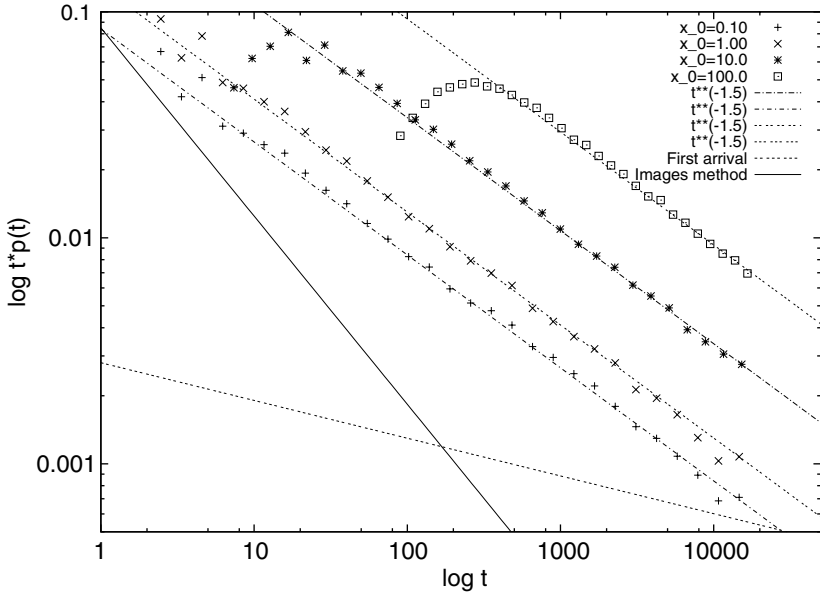


Figure 15. Numerical results for the first process time density process on the semi-infinite domain, for an Lévy flight with Lévy index $\alpha = 1.2$. Note abscissa, is $tp(t)$. For all initial conditions $x_0 = 0.10, 1.00, 10.0,$ and 100.0 the universal slope $-3/2$ in the $\log_{10}\text{-}\log_{10}$ plot is clearly reproduced, and it is significantly different from the two slopes predicted by the method of images and the direct definition of the first process time density.

Lévy stable indices α . Clearly, the scaling for the first arrival as well as the image method–first passage time density derived below are significantly different.

The following qualitative argument may be made in favor of the observed universality of the Lévy flight–first passage time density: The long-time decay is expected to be governed by short-distance jump events, corresponding to the central region of very small jump lengths for the Lévy stable jump length distribution. However, in this region the distribution function is, apart from a prefactor, indistinguishable from the Gaussian distribution, and therefore the long-time behavior should in fact be the same for any continuous jump length distribution $\lambda(x)$. In fact, the universal law (93) can only be modified in the presence of non-Markov effects such as broad waiting time processes or spatiotemporally coupled walks [45,46,70,80,81]. In terms of the special case covered by the theorem of Frisch and Frisch [75], in which the absorbing boundary coincides with the initial position, we can understand the general situation for finite $x_0 > 0$, as in the long-time limit, the distance x_0 becomes negligible in comparison to the diffusion length $\langle |x(t)| \rangle \sim t^{1/\alpha}$:

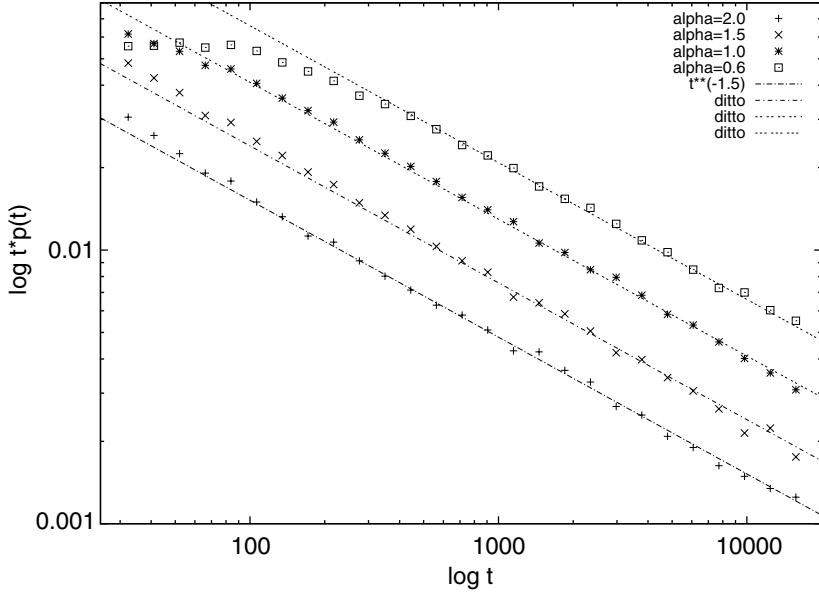


Figure 16. Same as in Fig. 15, for $\alpha = 2.0, 1.5, 1.0,$ and $0.6,$ and for the initial condition $x_0 = 10.0.$ Again, the universal $\sim t^{-3/2}$ behavior is obtained.

therefore the asymptotic behavior is necessarily governed by the same universality.

C. Inconsistency of Method of Images

We now demonstrate that the method of images produces a result, which is neither consistent with the universal behavior of the first passage time density (93) nor with the behavior of the PDF of first arrival (100), Given the initial condition $\delta(x - x_0),$ the solution $f_{im}(x, t)$ for the absorbing boundary value problem with the analogous Dirichlet condition $f_{im}(0, t) = 0$ according to the method of images is given in terms of the free propagator P by the difference [69,70]

$$f_{im}(x, t) = P(x - x_0, t) - P(x + x_0, t) \tag{101}$$

that is, a *negative* image solution originating at $-x_0$ balances the probability flux across the absorbing boundary. The corresponding pseudo-first passage time density is then calculated just as Eq. (95). For the image solution in the (k, u) domain, we obtain

$$f_{im}(k, u) = \frac{2i \sin(kx_0)}{u + D|k|^\alpha} \tag{102}$$

for a process which starts at $x_0 > 0$ and occurs in the right half-space. In u space, the image method–first passage time density becomes

$$p_{\text{im}}(u) = 1 - u \int_0^\infty dx \int_{-\infty}^\infty \frac{dk}{2\pi} e^{-ikx} \frac{2i \sin kx_0}{u + D|k|^\alpha} \quad (103)$$

After some transformations, we have

$$p_{\text{im}}(u) = 1 - \frac{2}{\pi} \int_0^\infty d\xi \frac{\sin(\xi s^{1/\alpha} x_0 / D^{1/\alpha})}{\xi(1 + \xi^\alpha)} \quad (104)$$

In the limit of small s , this expression reduces to $p_{\text{im}}(u) \sim 1 - \Lambda(\alpha)x_0 D^{-1/\alpha} u^{1/\alpha}$, with $\Lambda(\alpha) = (2/\pi) \int_0^\infty (1 + \xi^\alpha)^{-1} d\xi = 2/(\alpha \sin(\pi/\alpha))$. In like manner, we find the long- t form

$$p_{\text{im}}(t) \sim 2\Gamma(1/\alpha) \frac{x_0}{\pi\alpha D^{1/\alpha} t^{1+1/\alpha}} \quad (105)$$

for the image method–first passage time density. In the Gaussian limit $\alpha = 2$, expression (105) produces $p_{\text{im}}(t) \sim x_0/\sqrt{4\pi Dt^3}$, in accordance with Eq. (97). Conversely, for general $1 < \alpha < 2$, $p(t)$ according to Eq. (105) would decay faster than $\sim t^{-3/2}$. The failure of the method of images is closely related to the strongly nonlocal character of Lévy flights. Under such conditions, the random variable $x - x_0$ is no longer independent of $x + x_0$, so that the method of images is not appropriate.

The proper dynamical formulation of a Lévy flight on the semi-infinite interval with an absorbing boundary condition at $x = 0$, and thus the determination of the first passage time density, has to ensure that in terms of the random walk picture jumps across the sink are forbidden. This objective can be consistently achieved by setting $f(x, t) \equiv 0$ on the left semi-axis, i.e., actually removing the particle when it crosses the point $x = 0$. This procedure formally corresponds to the modified dynamical equation

$$\frac{\partial f(x, t)}{\partial t} = \frac{D}{\kappa} \frac{\partial^2}{\partial x^2} \int_0^\infty \frac{f(x', t)}{|x - x'|^{\alpha-1}} dx' \equiv \frac{\partial^2}{\partial x^2} \mathcal{F}(x, t) \quad (106)$$

in which the fractional integral is confined to the semi-infinite interval. Here, we have written

$$\kappa = 2\Gamma(2 - \alpha) \left| \cos \frac{\pi\alpha}{2} \right| \quad (107)$$

After Laplace transformation and integrating over x twice, one obtains

$$\int_0^{\infty} K(x-x', u) f(x', u) dx' = (x-x_0)\Theta(x-x_0) - xp(u) - \mathcal{F}(0, u) \quad (108)$$

where $p(t)$ is the FPTD and the kernel $K(x, u) = ux\Theta(x) - (\kappa|x|^{\alpha-1})$. This equation is formally a Wiener–Hopf equation of the first kind [82]. After some manipulations similar to those applied in Ref. 76, we arrive at the asymptotic expression

$$p(u) \simeq 1 - Cu^{1/2}, \quad \text{where } C = \text{const} \quad (109)$$

in accordance with the expected universal behavior (93) and with the findings of reference [76]. Thus, the dynamic equation (106) governs the first passage time density problem for Lévy flights. We note that due to the truncation of the fractional integral it was not possible to modify the well-established Grünwald–Letnikov scheme [61] to numerically solve Eq. (106) with enough computational efficiency to obtain the direct solution for $f(x, t)$.

V. BARRIER CROSSING OF A LÉVY FLIGHT

The escape of a particle from a potential well is a generic problem investigated by Kramers [84] that is often used to model chemical reactions, nucleation processes, or the escape from a potential well [84]. Keeping in mind that many stochastic processes do not obey the central limit theorem, the corresponding Kramers escape behavior will differ. For subdiffusion, the temporal evolution of the survival behavior is bound to change, as discussed in Ref. 85. Here, we address the question how the stable nature of Lévy flight processes generalizes the barrier crossing behavior of the classical Kramers problem [86]. An interesting example is given by the α -stable noise-induced barrier crossing in long paleoclimatic time series [87]; another new application is the escape from traps in optical or plasma systems (see, for instance, Ref. 88).

A. Starting Equations

Here, we investigate barrier crossing processes in a reaction coordinate $x(t)$ governed by a Langevin equation [Eq. (25)] with white Lévy noise $\Gamma_{\alpha}(t)$. Now, however, the external potential $V(x)$ is chosen as the (typical) double-well shape

$$V(x) = -\frac{a}{2}x^2 + \frac{b}{4}x^4 \quad (110)$$

compare, for instance, Ref. 89. For convenience, we introduce dimensionless variables $t \rightarrow t/t_0$ and $x \rightarrow x/x_0$ with $t_0 = m\eta/a$ and $x_0^2 = 1/(bt_0)$ and

dimensionless noise strength $D \rightarrow Dt_0^{1/\alpha}/x_0$ (by $\Gamma_\alpha(t_0t) \rightarrow t_0^{1/\alpha-1}\Gamma_\alpha(t)$) [43], so that we have the stochastic equation

$$\frac{dx(t)}{dt} = (x - x^3) + D^{1/\alpha}\Gamma_\alpha(t) \tag{111}$$

Here, we restrict our discussion to $1 \leq \alpha < 2$.

B. Brownian Motion

In normal Brownian motion corresponding to the limit $\alpha = 2$, the survival probability S of a particle whose motion at time $t = 0$ which is initiated in one of the potential minima $x_{\min} = \pm 1$, follows an exponential decay $\mathcal{S}(t) = \exp(-t/T_c)$ with mean escape time T_c , such that the probability density function $p(t) = -d\mathcal{S}/dt$ of the barrier crossing time t becomes

$$p(t) = T_c^{-1} \exp(-t/T_c) \tag{112}$$

The mean crossing time (MCT) follows the exponential law

$$T_c = C \exp(h/D) \tag{113}$$

where h is the barrier height (equal to $1/4$ for the potential (110)) in rescaled variables, and the prefactor C includes details of the potential [84]. We want to determine how the presence of Lévy stable noise modifies the laws (112) and (113).

C. Numerical Solution

The Langevin equation [Eq. (111)] was integrated numerically following the procedure developed in Ref. 90. Whence, we obtained the trajectories of the particle shown in Fig. 17. In the Brownian limit, we reproduce qualitatively the behavior found in Ref. 89. Accordingly, the fluctuations around the positions of the minima are localized in the sense that their width is clearly smaller than the distance between the minima and barrier. In contrast, for progressively smaller stable index α , characteristic spikes become visible, and the individual sojourn times in one of the potential wells decrease. In particular, we note that single spikes can be of the order of or larger than the distance between the two potential minima.

From such single trajectories we determine the individual barrier crossing times as the time interval between a jump into one well across the zero line $x = 0$ and the escape across $x = 0$ back to the other well. In Fig. 18, we demonstrate that on average, the crossing times are distributed exponentially, and thus follow the same law (112) already known from the Brownian case. Such a result has been reported in a previous study of Kramers' escape driven by Lévy noise [91]. In fact, the exponential decay of the survival probability

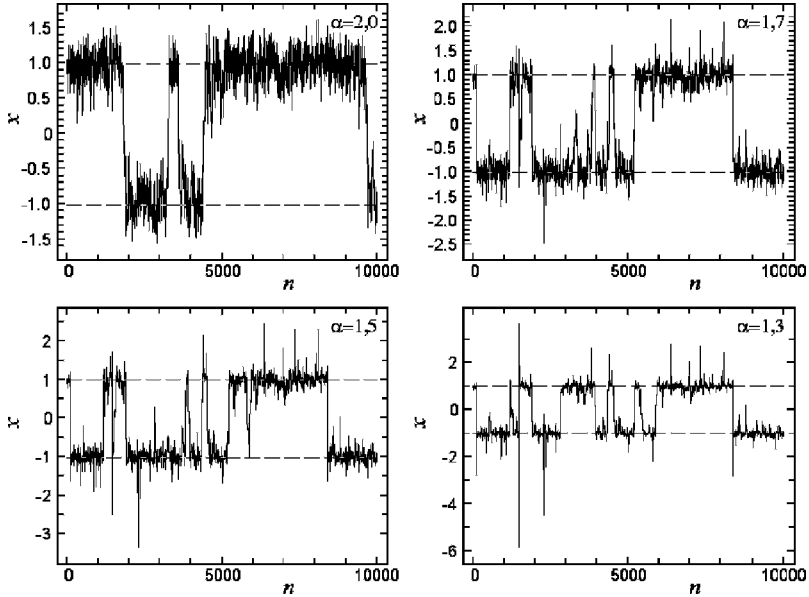


Figure 17. Typical trajectories for different stable indexes α obtained from numerical integration of the Langevin equation [Eq. (111)]. The dashed lines represent the potential minima at ± 1 . In the Brownian case $\alpha = 2$, previously reported behavior is recovered [89]. In the Lévy stable case, occasional long jumps of the order of or larger than the separation of the minima can be observed. Note the different scales.

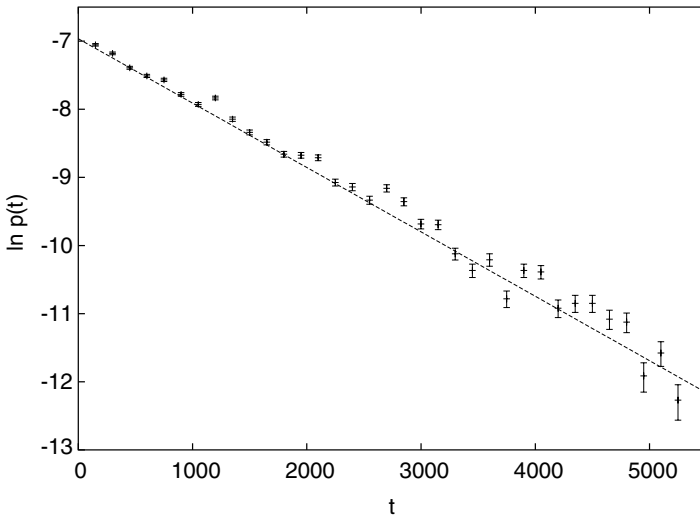


Figure 18. Probability density function $p(t)$ of barrier crossing times for $\alpha = 1.0$ and $D = 10^{-2.5} \approx 0.00316$. The dashed line is a fit to Eq. (112) with mean crossing time $T_c = 1057.8 \pm 17.7$.

S observed in a Lévy flight is not surprising, given the Markovian nature of the process. Due to the Lévy stable properties of the noise Γ_α , the Langevin equation [Eq. (111)] produces occasional long jumps, by which the particle can cross the barrier. Large enough values of the noise Γ_α thus occur considerably more frequently than in the Brownian case with Gaussian noise ($\alpha = 2$), causing a lower mean crossing time.

The numerical integration of the Langevin equation (111) was repeated for various stable indices α , and for a range of noise strengths D . From these simulations we obtain the detailed dependence of the mean crossing time $T_c(\alpha, D)$ on both of the parameters, α and D . As expected, for decreasing noise strength, the mean crossing time increases. For sufficiently large values of $1/D$ and fixed α , a power-law trend in the double-logarithmic plot is clearly visible. These power-law regions, for the investigated range of α are in very good agreement with the analytical form

$$T_c(\alpha, D) = \frac{C(\alpha)}{D^{\mu(\alpha)}} \tag{114}$$

over a large range of D . Equation (114) is the central result of this study. It is clear from Fig. 19, that this relation is appropriate for the entire α -range studied

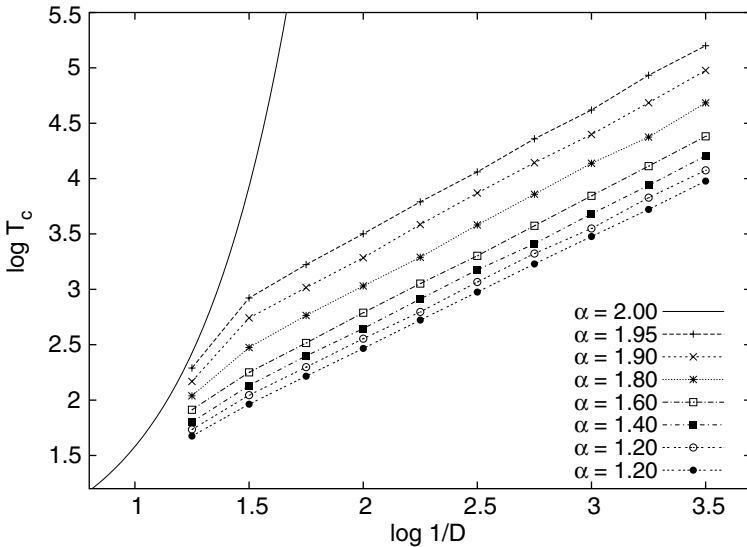


Figure 19. Escape time T_c as a function of noise strength D for various α . Above roughly $\lg 1/D = 1.5$, a power-law behavior is observed that corresponds to Eq. (114). The curve [Eq. (113)] for $\alpha = 2.0$ appears to represent a common envelope.

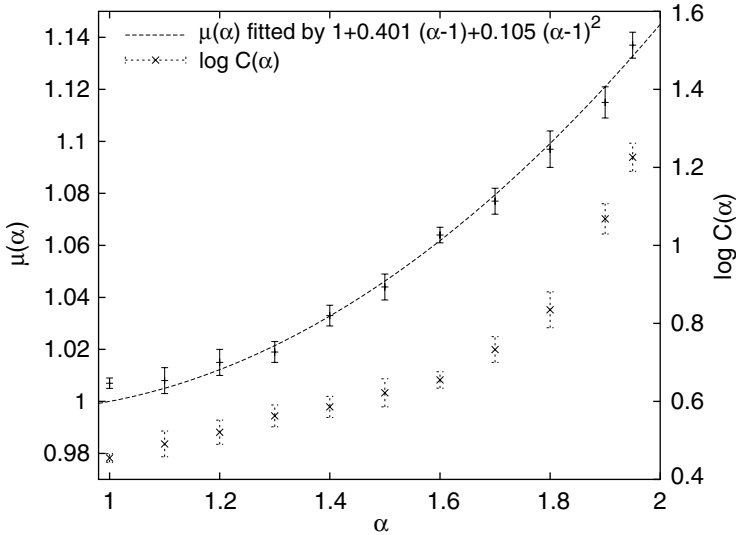


Figure 20. Scaling exponent μ as function of stable index α . The constant behavior $\mu(\alpha) \approx 1$ over the range $1 \leq \alpha \lesssim 1.6$ is followed by an increase above 1.6, and it eventually shows an apparent divergence close to $\alpha = 2$, where Eq. (113) holds. Corresponding to the right ordinate, we also plot the decadic logarithm of the amplitude $C(\alpha)$.

in our simulations. For larger noise strength, we observe a breakdown of the power-law trend, and the curves seem to approach the mean crossing time behavior of the Brownian process ($\alpha = 2$) as a common envelope. A more thorough numerical analysis of this effect will be necessary in order to ascertain its exact nature. The main topic we want to focus on here is the behavior embodied in Eq. (114). We note from Fig. 19 that for α ranging roughly between the Cauchy case $\alpha = 1$ and the Holtzmark case $\alpha = 3/2$, the exponent μ is almost constant; that is, the corresponding lines in the log-log plot are almost parallel. The behavior of both the scaling exponent μ and the prefactor C as a function of the stable index α becomes clear in Fig. 20. There, we recognize a slow variation of μ for values of α between $3/2$ and slightly below 2, before a steeper rise in close vicinity of 2. This apparent divergence must be faster than any power, so that in the Gaussian noise limit $\alpha = 2$, the activation follows the exponential law (113) instead of the scaling form (114). The $\mu(\alpha)$ results are fitted with the parabola indicated in the plot where, for the analytical results derived below, we forced the fit function to pass through the point $\mu(1) = 1$.

D. Analytical Approximation for the Cauchy Case

In the Cauchy limit $\alpha = 1$, we can find an approximate result for the mean crossing time as a function of noise strength D . To this end, we start with the

rescaled fractional Fokker–Planck equation [20,46,54,57,71], corresponding to equation (111),

$$\frac{\partial P(x, t)}{\partial t} = \frac{\partial}{\partial x} (-x + x^3)P(x, t) + D \frac{\partial^\alpha}{\partial |x|^\alpha} P(x, t) \tag{115}$$

Rewriting Eq. (115) in continuity equation form $\partial P(x, t)/\partial t + \partial j(x, t)/\partial x = 0$, that is equivalent to $\partial P(k, t)/\partial t = ikj(k, t)$ in k space, we obtain for the flux the expression

$$j(k) = \left(-\frac{\partial^3}{\partial k^3} - i \frac{\partial}{\partial k} + iD \operatorname{sign}(k)|k|^{\alpha-1} \right) P(k, t) \tag{116}$$

To obtain an approximate expression for the mean crossing time, we follow the standard steps [92] and for large values of $1/D$ make the constant flux approximation assuming that the flux across the barrier is a constant, j_0 , corresponding to the existence of a stationary solution $P_{st}(x)$. By integration of the continuity equation, it then follows that equation (112) is satisfied, and $T_c = 1/j_0$. Due to the low noise strength, we also assume that for all relevant times the normalization $\int_{-\infty}^0 P_{st}(x) dx = 1$ obtains.

In this constant flux approximation, we obtain from equation (116) the relation

$$\frac{d^3 P_{st}(k)}{dk^3} + \frac{dP_{st}(k)}{dk} - D \operatorname{sign}(k)P_{st}(k) = 2\pi i j_0 \delta(k) \tag{117}$$

in the Cauchy case $\alpha = 1$. With the ansatz $P_{st}(k) = C_1 e^{z^\pm k} + C_2 e^{(z^*)^\pm k}$ for $k \gtrless 0$, we find the characteristic equation $(z^\pm)^3 + z^\pm \mp D = 0$ solved by the Cardan expressions $z^\pm = -\frac{1}{2}(u_\pm + v_\pm) + \frac{1}{2}i\sqrt{3}(u_\pm - v_\pm)$, with $u_\pm^3 = D(1 + \sqrt{1 + 4/[27D^2]})/2 = -v_\mp^3$ and $v_\pm^3 = D(1 - \sqrt{1 + 4/[27D^2]})/2 = -u_\mp^3$. Matching the left and right solutions at $k = 0$, requiring that $P_{st}(k) \in \mathbb{R}$, and assuming that $P_{st}(k)$ in the constant flux approximation is far from the fully relaxed ($t \rightarrow \infty$) solution, we obtain the shifted Cauchy form

$$P_{st}(k) = \frac{j_0}{2\zeta_+ \zeta_-} \frac{\zeta_+}{(x + \zeta_-)^2 + \zeta_+^2},$$

$$\therefore \zeta_+ = \frac{1}{2}(u_+ + v_+), \quad \zeta_- = \frac{\sqrt{3}}{2}(u_+ - v_+) \tag{118}$$

With the normalization $\int_{-\infty}^0 P_{st}(x) dx = 1$, we arrive at the mean crossing time

$$T_c = \frac{\pi}{4\zeta_+ \zeta_-} \left(1 + \frac{2}{\pi} \arctan \frac{\zeta_-}{\zeta_+} \right) \tag{119}$$

For $D \ll 1$, $\zeta_+ \approx D/2$ and $\zeta_- \approx 1$, so that $T_c \approx \pi/D$. In comparison with the numerical result corresponding to Fig. 18 with $T_c = 1057.8$ for $D = 0.00316$, we calculate from our approximation $T_c \approx 994.2$, which is within 6% of the numerical result. This good agreement also corroborates the fact that the constant flux approximation appears to pertain to Lévy flights.

E. Discussion

We observe from numerical simulations an exponential decrease of the survival probability $\mathcal{S}(t)$ in the potential well, at the bottom of which we initialize the process. Moreover, we find that the mean crossing time assumes the scaled form (114) with scaling exponent μ being approximately constant in the range $1 \leq \alpha \lesssim 1.6$, followed by an increase before the apparent divergence at $\alpha = 2$, that leads back to the exponential form of the Brownian case, Eq. (113). An analytic calculation in the Cauchy limit $\alpha = 1$ reproduces, consistently with the constant flux approximation commonly applied in the Brownian case, the scaling $T_c \sim 1/D$, and, within a few percent error, the numerical value of the mean crossing time T_c .

Employing scaling arguments, we can restore the dimensionality into expression (114) for the mean crossing time. From our model potential (110), where we absorb the friction factor $m\eta$ via $a \rightarrow a/(m\eta)$ and $b \rightarrow b/(m\eta)$, we find that the minima are $x_{\min} = \pm\sqrt{a/b}$ and the barrier height $\Delta V = a^2/(4b)$. In terms of the rescaled prefactors a and b with dimensions $[a] = \text{sec}^{-1}$ and $[b] = \text{sec}^{-1}\text{cm}^{-2}$, we can now reintroduce the dimensions via $t_0 = 1/a$ and $x_0^2 = b/a$. In the domain where $T_c \sim 1/D$ (i.e., $\mu(\alpha) \approx 1$), we then have the scaling

$$T_c \sim \frac{x_0^\alpha}{D} = \frac{(a/b)^{\alpha/2}}{D} = \frac{|x_{\min}|^\alpha}{D} \quad (120)$$

by analogy with the result reported in Ref. 91. However, we emphasize two caveats based on our results: (i) The linear behavior in $1/D$ is not valid over the entire α -range. For larger values, $\alpha \gtrsim 1.6$, the scaling exponent $\mu(\alpha)$ assumes nontrivial values; then, the simple scaling used to establish Eq. (120) has to be modified. It is not immediately obvious how this should be done systematically. (ii) From relation (120) it cannot be concluded that the mean crossing time is independent of the barrier height ΔV , despite the fact that T_c depends on the distance $|x_{\min}|$ from the barrier only. The latter statement is obvious from the expressions for x_{\min} and ΔV derived for our model potential: The location of the minima relative to the barrier is in fact coupled to the barrier height. Therefore, a random walker subject to Lévy noise senses the potential barrier and does not simply move across it with the characteristic time given by the free mean-square displacement. Apparently, the activation for the mean crossing time as a function of noise strength D varies only as a power law instead of the standard exponential behaviour.

The time dependence of the probability density $-d\mathcal{P}(t)/dt$ for first barrier crossing time of a Lévy flight process is exponential, just as the standard Brownian case. This can be understood qualitatively because the process is Markovian. From the governing dynamical equation (115), it is clear that the relaxation of modes is exponential, compare Ref. 46. For low noise strength D , the barrier crossing will be dominated by the slowest time-eigenmode $\simeq e^{-\lambda_1 t}$ with eigenvalue λ_1 . This is indeed similar to the first passage time problem of Lévy flights discussed in the previous section.

VI. DISSIPATIVE NONLINEARITY

The alleged “pathology” of Lévy flights is related to their divergent variance, unless confined by a steeper than harmonic external potential. There indeed exist examples of processes where the diverging variance does not pose a problem: for example, diffusion in energy space [93], or the Lévy flight in the chemical coordinate of diffusion along a polymer chain in solution, where Lévy jump length statistics are invoked by intersegmental jumps, which are geometrically short in the embedding space [94]. Obviously however, for a particle with a finite mass moving in Euclidian space, the divergence of the variance is problematic.⁷

There are certain ways of overcoming this difficulty: (i) by a time cost through coupling between x and t , producing Lévy walks [45,98], or (ii) by a cutoff in the Lévy noise to prevent divergence [99,100]. While (i) appears a natural choice, it gives rise to a nonMarkov process. Conversely, (ii) corresponds to an *ad hoc* measure.

A. Nonlinear Friction Term

Here, we pursue an alternative, physical way of dealing with the divergence; namely, inclusion of nonlinear dissipative terms. They provide a mechanism, that naturally regularizes the Lévy stable PDF $P(V, T)$ of the velocity distribution. Dissipative nonlinear structures occur naturally for particles in a frictional environment at higher velocities [101]. A classical example is the Riccati equation $Mdv(t)/dt = Mg - Kv(t)^2$ for the motion of a particle of mass M in a gravitational field with acceleration g [102], autonomous oscillatory systems with a friction that is nonlinear in the velocity [101,103], or nonlinear corrections to the Stokes drag as well as drag in turbulent flows [104]. The occurrence of a non-constant friction coefficient $\gamma(V)$ leading to a nonlinear dissipative force

⁷Note that in fact the regular diffusion equation includes a similar flaw, although less significant: Due to its parabolic nature, it features an infinite propagation speed; that is, even at very short times, there exists a finite value of $P(x, t)$ for large $|x|$. In that case, this can be removed by invoking the telegrapher’s (Cattaneo) equation [95–97]. (*Editor’s note:* For a critical discussion of this procedure, see Risken [12, p. 257 *et seq.*])

$-\gamma(V)V$ was highlighted in Klimontovich's theory of nonlinear Brownian motion [105]. In what follows, we show that dissipative nonlinear structures regularize a stochastic process subject to Lévy noise, leading to finite variance of velocity fluctuations and thus a well-defined kinetic energy. The velocity PDF $P(V, t)$ associated with this process preserves the properties of the Lévy process for smaller velocities; however, it decays faster than a Lévy stable density and thus possesses a physical cutoff. In what follows, we start with the asymptotic behavior for large V and then address the remaining, central part of $P(V, T)$, that preserves the Lévy stable density property.

B. Dynamical Equation with Lévy Noise and Dissipative Nonlinearity

The Langevin equation for a random process in the velocity coordinate V is usually written as [59]

$$\frac{dV(t)}{dt} + \gamma(V)V(t) = \Gamma_\alpha(t) \quad (121)$$

with the constant friction $\gamma_0 = \gamma(0)$. $\Gamma_\alpha(t)$ is the α -stable Lévy noise defined in terms of a characteristic function (see Section I). The characteristic function of the velocity PDF $P(V, t)$, $P(k, t) \equiv \mathcal{F}\{P(V, t)\}$ is then governed by the dynamical equation [59]

$$\frac{\partial P(k, t)}{\partial t} = -\gamma_0 k \frac{\partial P(k, t)}{\partial k} - D|k|^\alpha P(k, t) \quad (122)$$

This is exactly the V -space equivalent of the Lévy flight in an external harmonic potential discussed in the introduction. Under stationary conditions the characteristic function assumes the form

$$P_{st}(k, t) = \exp\left(-\frac{D|k|^\alpha}{\gamma_0 \alpha}\right) \quad (123)$$

So that the PDF $P(V, t)$ converges toward a Lévy stable density of index α . This stationary solution possesses, however, a diverging variance.

To overcome the divergence of the variance $\langle V^2(t) \rangle$, we introduce into Eq. (121) the velocity-dependent dissipative nonlinear form $\gamma(V)$ for the friction coefficient [101,105]. We require $\gamma(V)$ to be symmetric in V [105], assuming the virial expansion up to order $2N$

$$\gamma(V) = \gamma_0 + \gamma_2 V^2 + \dots + \gamma_{2N} V^{2N} \quad \therefore \gamma_{2N} > 0 \quad (124)$$

The coefficients γ_{2n} are assumed to decrease rapidly with growing n ($n \in \mathbb{N}$). To determine the asymptotic behavior, it is sufficient to retain the highest power $2N$.

More generally, we will consider a power $\gamma_v|V|^v$ with $v \in R^+$ and $\gamma_v > 0$. We will show that, despite the input driving Lévy noise, the inclusion of the dissipative nonlinearity (124) ensures that the resulting process possesses a finite variance.

To this end, we pass to the kinetic equation for $P(V, t)$, the fractional Fokker–Planck equation [20,46,54,60,64]

$$\frac{\partial P(V, t)}{\partial t} = \frac{\partial}{\partial V}(V\gamma(V)P(V, t)) + D \frac{\partial^\alpha P(V, t)}{\partial |V|^\alpha} \quad (125)$$

The nonlinear friction coefficient $\gamma(V)$ thereby takes on the role of a confining potential: while for $\gamma_0 = \gamma(0)$ the drift term $V\gamma_0$, as mentioned before, is just the restoring force exerted by the harmonic Ornstein–Uhlenbeck potential, the next higher-order contribution $\gamma_2 V^3$ corresponds to a quartic potential, and so forth. The fractional operator $\partial^\alpha/\partial |V|^\alpha$ in Eq. (125) for the velocity coordinate for $1 < \alpha < 2$ is explicitly given by [20,64]

$$\frac{d^\alpha P(V)}{d|V|^\alpha} = -\kappa \frac{d^2}{dV^2} \int_{-\infty}^{\infty} \frac{P(V')}{|V - V'|^{\alpha-1}} dV' \quad (126)$$

by analogy with the x -domain operator (31), with κ being defined in Eq. (107).

C. Asymptotic Behavior

To derive the asymptotic behavior of $P(V, t)$ in the presence of a particular form of $\gamma(V)$, it is sufficient to consider the highest power, say, $\gamma(V) \sim \gamma_v|V|^v$. In particular, to infer the behavior of the stationary PDF $P_{\text{st}}(V)$ for $V \rightarrow \infty$, it is reasonable to assume that we can truncate the integral $\int_{-\infty}^{\infty} dV'$ in the fractional operator (126) at the pole $V' = V$, since the domain of integration for the remaining left-side operator is much larger than the cutoff right-side domain. Moreover, the remaining integral over $(-\infty, V]$ also contains the major portion of the PDF. For $V \rightarrow +\infty$, we find in the stationary state after integration over V ,

$$\gamma_v V^{v+1} P_{\text{st}}(V) \simeq D\kappa \frac{d}{dV} \int_{-\infty}^V \frac{P_{\text{st}}(V')}{(V - V')^{\alpha-1}} dV' \quad (127)$$

We then use the ansatz $P_{\text{st}}(V) \sim C/|V|^\mu$, $\mu > 0$. With the approximation $\int_{-\infty}^V P_{\text{st}}(V')/(V - V')^{\alpha-1} dV' \sim V^{1-\alpha} \int_{-\infty}^V P_{\text{st}}(V') dV' \sim V^{1-\alpha} \int_{-\infty}^{\infty} P_{\text{st}}(V') dV' = V^{1-\alpha}$ we obtain the asymptotic form

$$P_{\text{st}}(V) \simeq \frac{C_\alpha D}{\gamma_v |V|^\mu} \quad \therefore \mu = \alpha + v + 1 \quad (128)$$

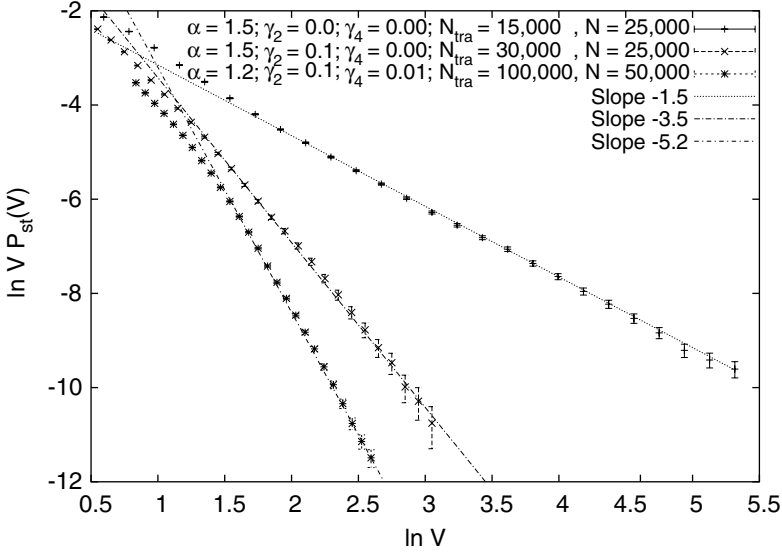


Figure 21. Power-law asymptotics of the stationary PDF, ln–ln scale. We observe the expected scaling with exponent μ from Eq. (128). In the graph, we also indicate the number N_{tra} of trajectories of individual length N simulated to produce the average PDF.

valid for $V \rightarrow \pm\infty$ due to symmetry. We conclude that for all $v > v_{\text{cr}} = 2 - \alpha$ the variance $\langle V^2 \rangle$ is finite, and thus a dissipative nonlinearity whose highest power v exceeds the critical value v_{cr} counterbalances the energy supplied by the Lévy noise $\Gamma_\alpha(t)$.

D. Numerical Solution of Quadratic and Quartic Nonlinearity

Let us consider dissipative nonlinearity up to the quartic order contribution, $\gamma(V) = \gamma_0 + \gamma_2 V^2 + \gamma_4 V^4$. According to the previous result (128), the stationary PDF for the quadratic case with $\gamma_2 > 0$ and $\gamma_4 = 0$ falls off like $P_{\text{st}}(V) \sim |V|^{-\alpha-3}$, and thus $\forall \alpha \in (0, 2)$ the variance $\langle V^2 \rangle$ is finite. Higher-order moments such as the fourth-order moment $\langle V^4 \rangle$ are, however, still infinite. In contrast, if $\gamma_4 > 0$, the fourth-order moment is finite. We investigate this behavior numerically by solving the Langevin equation (121); compare Ref. 64 for details.

In Fig. 21 we show the asymptotic behavior of the stationary PDF $P_{\text{st}}(V)$ for three different sets of parameters. Clearly, in all three cases the predicted power-law decay is obtained, with exponents that, within the estimated error bars agree well with the predicted relation for μ according to Eq. (128).⁸

⁸From the scattering of the numerical data after repeated runs, see Fig. 7.

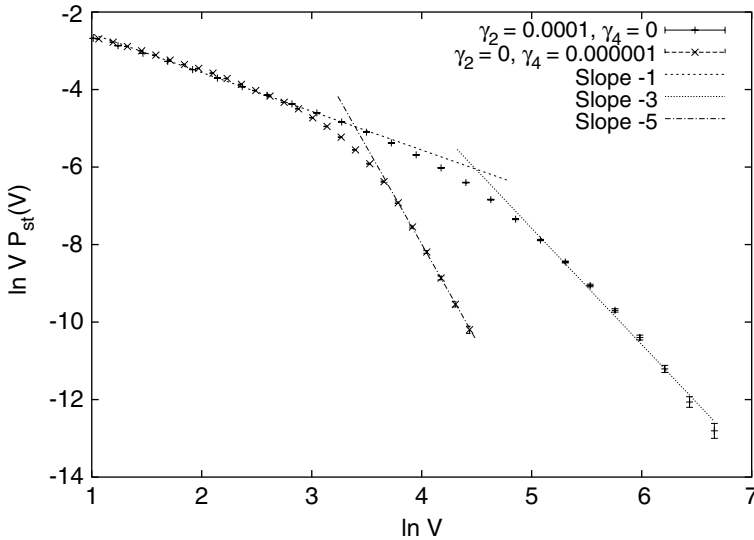


Figure 22. Stationary PDF $P_{st}(V)$ for $\gamma_0 = 1.0$ and (i) $\gamma_2 = 0.0001$ and $\gamma_4 = 0$, and (ii) $\gamma_2 = 0$ and $\gamma_4 = 0.000001$, with $\alpha = 1.0$. The lines indicate the slopes -1 , -3 , and -5 .

E. Central Part of $P(V, t)$

The nonlinear damping (124) mainly affects larger velocities, while smaller velocities ($V \ll 1$) are mainly subject to the lowest-order friction $\gamma(0)$. We therefore expect that in the central region close to $V = 0$, the PDF $P(V, T)$ preserves its Lévy stable density character. This is demonstrated in Fig. 22, where the initial power-law decay of the Lévy stable density eventually gives way to the steeper decay caused by the nonlinear friction term. In general, the PDF shows transitions between multiple power laws in the case when several higher-order friction terms are retained. The turnover point from the unaffected Lévy stable density to steeper decay caused by nonlinear friction depends on the ratio $\gamma_0 : \gamma_{2n}$, where $2n$ is the next higher-order nonvanishing friction coefficient.

In Fig. 23, we show the time evolution of the variance $\langle V^2(t) \rangle$ for various combinations of Lévy index α and magnitude γ_2 of the quadratic nonlinearity ($\gamma_0 = 1.0$ and $\gamma_4 = 0.0$). For all cases with finite γ_2 ($\gamma_2 = 0.1$), we find convergence of the variance to a stationary value. For the two smaller α values (1.2 and 1.5), we observe some fluctuations; however, these are comparatively small with respect to the stationary value they oscillate around. For $\alpha = 1.8$, the fluctuations are hardly visible, and in fact the stationary value is practically the same as in the Gaussian case $\alpha = 2.0$. In contrast, the case with vanishing

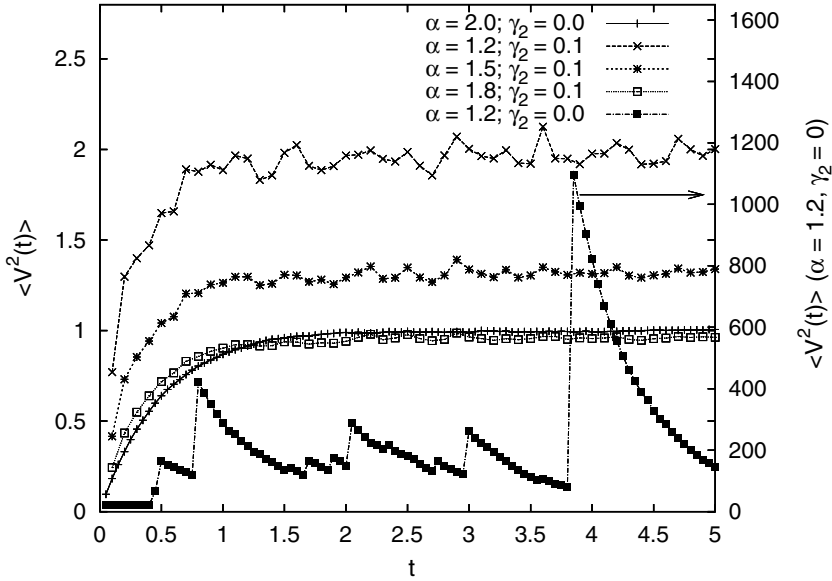


Figure 23. Variance $\langle V^2(t) \rangle$ as function of time t , with the quartic term set to zero, $\gamma_4 = 0$ and $\gamma_0 = 1.0$ for all cases. The variance is finite for the cases $\alpha = 2.0, \gamma_2 = 0.0$; $\alpha = 1.2, \gamma_2 = 0.1$; $\alpha = 1.5, \gamma_2 = 0.1$; and $\alpha = 1.8, \gamma_2 = 0.1$. These correspond to the left ordinate. For the case $\alpha = 1.2, \gamma_2 = 0.0$, the variance diverges and strong fluctuations are visible; note the large values of this curve corresponding to the right ordinate.

γ_2 (and $\alpha = 1.2$) clearly shows large fluctuations requiring a right ordinate whose span is roughly two orders of magnitude larger than that of the left ordinate.

Similarly, in Fig. 24, we show the fourth order moment $\langle V^4(t) \rangle$ as a function of time. It is obvious that only for finite γ_4 ($\gamma_4 = 0.01$ and $\alpha = 1.8$) the moment converges to a finite value that is quite close to the value for the Gaussian case ($\alpha = 2.0$) for which all moments converge. In contrast to this behavior, both examples with vanishing γ_4 exhibit large fluctuations. These are naturally much more pronounced for smaller Lévy index ($\alpha = 1.2$, corresponding to the right ordinate).

F. Discussion

Strictly speaking, all naturally occurring power-laws in fractal or dynamic patterns are finite. Scale-free models nevertheless provide an efficient description of a wide variety of processes in complex systems [16,20,46,106]. This phenomenological fact is corroborated by the observation that the power-law properties of Lévy processes persist strongly even in the presence of cutoffs [99]

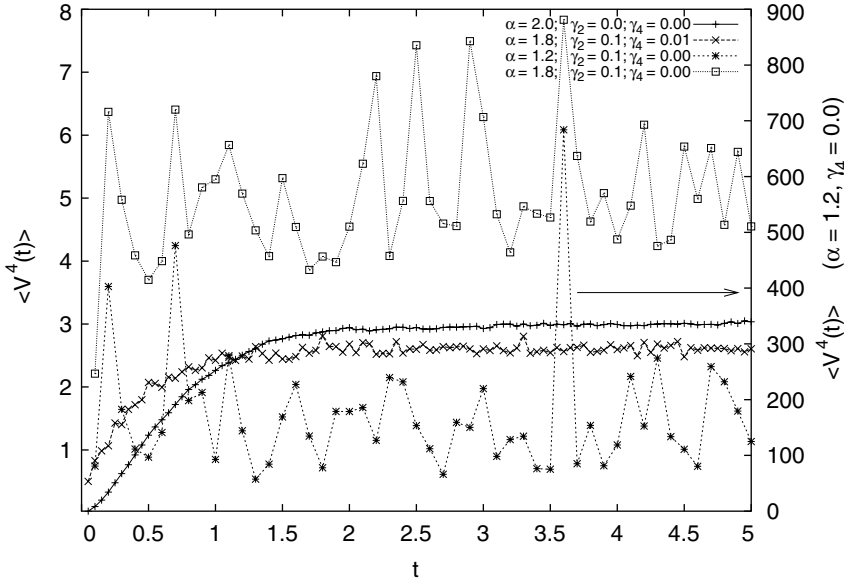


Figure 24. Fourth-order moment $\langle V^4(t) \rangle$ as function of t , with $\gamma_0 = 1$. $\langle V^4(t) \rangle$ converges to a finite value for the two cases $\alpha = 2$ (Gaussian) and $\alpha = 1.8$ with $\gamma_4 = 0.01$. The other two examples with vanishing quartic contribution ($\gamma_4 = 0$) show large fluctuations—that is, diverging $\langle V^4(t) \rangle$. Note that the case $\alpha = 1.2$ and $\gamma_4 = 0$ corresponds to the right ordinate.

and, mathematically, by the existence of the generalized central limit theorem due to which Lévy stable laws become fundamental [69]. A categorical question is whether in the presence of Lévy noise, there exists a physical cause to remove the consequential divergences. A possible, physically reasonable answer is given by introducing a nonconstant friction coefficient $\gamma(V)$, as occurs in various classical systems. Here, we present a concise derivation of the regularization of a stochastic process in velocity space driven by Lévy stable noise, in the presence of dissipative nonlinearities.

These dissipative nonlinearities remove the divergence of the kinetic energy from the measurable subsystem of the random walker. In idealized mathematical language, the surrounding heat bath provides an infinite amount of energy through the Lévy noise, and the coupling via the nonlinear friction dissipates an infinite amount of energy into the bath, and thereby introduces a natural cutoff in the kinetic energy distribution of the random walker subsystem. Physically, such divergences are not expected, but correspond to the limiting behavior associated with large numbers in probability theory. In this section, we showed that both statements can be reconciled, and that Lévy processes are indeed physical.

VII. SUMMARY

A hundred years after Einstein's seminal work [4], the theory of stochastic processes has been put on solid physical and mathematical foundations, at the same time playing a prominent role in many branches of science [36,107–109].

Lévy flights represent a widely used tool in the description of anomalous stochastic processes. By their mathematical definition, Lévy flights are Markovian and their statistical limit distribution emerges from independent identically distributed random variables, by virtue of the central limit theorem. Despite this quite straightforward definition, Lévy flights are less well understood than one might at first assume. This is due to their strongly nonlocal character in space, these long-range correlations spanning essentially the entire available geometry; as exemplified by the infinite range of the integration boundaries in the associated fractional operator.

In this review, we have addressed some of the fundamental properties of random processes, these being the behaviour in external force fields, the first passage and arrival behaviour, as well as the Kramers-like escape over a potential barrier. We have examined the seemingly pathological nature of Lévy flights and showed that dissipative non-linear mechanisms cause a natural cutoff in the PDF, so that with a finite experimental range the untruncated Lévy flight still provides a good description.

These investigations have been almost entirely based on fractional diffusion and Fokker–Planck equations with a fractional Riesz derivative and have turned out to be a convenient basis for mathematical manipulations, while at the same time being easy to interpret in the context of a dynamical approach.

Acknowledgments

We would like to thank Iddo Eliazar and Igor M. Sokolov for helpful discussions.

VIII. APPENDIX. NUMERICAL SOLUTION METHODS

In this appendix, we briefly review the numerical techniques, which have been used in this work to determine the PDF from the fractional Fokker–Planck equation [Eq. (38)] and the Langevin equation [Eq. (37)].

A. Numerical solution of the fractional Fokker–Planck equation [Eq. (38)] via the Grünwald–Letnikov Method

From a mathematical point of view, the fractional Fokker–Planck equation [Eq. (38)] is an first-order partial differential equation in time, and of nonlocal, integrodifferential kind in the position coordinate x . It can be solved numerically via an efficient discretization scheme following Grünwald and Letnikov [110–112].

Let us designate the force component on the right-hand side of Eq. (38) as

$$\bar{F}(x, t) \equiv \frac{\partial}{\partial x} \left(\frac{dV}{dx} P \right) \tag{129}$$

and the diffusion part as

$$\bar{D}(x, t) \equiv \frac{\partial^\alpha P}{\partial |x|^\alpha} \tag{130}$$

With these definitions, we can rewrite Eq. (38) in terms of a discretisation scheme as

$$\frac{P_{j,n+1} - P_{j,n}}{\Delta t} = \bar{F}_{j,n} + \bar{D}_{j,n} \tag{131}$$

where we encounter the term

$$\bar{F}_{j,n} = x_j^{c-2} \left[(c-1)P_{j,n} + x_j \frac{P_{j+1,n} - P_{j-1,n}}{2\Delta x} \right] \tag{132}$$

which is the force component of the potential $V(x) = |x|^c/c$. Here, Δt and Δx are the finite increments in time and position, such that $t_n = n\delta t$ and $x_j = j\Delta x$, for $n = 0, 1, \dots, N$ and $j = 0, 1, \dots, J$, and $P_{j,n} \equiv P(x_j, t_n)$. Due to the inversion symmetry of the kinetic equation (38), it is sufficient to solve it on the right semi-axis. In the evaluation of the numerical scheme, we define x_J such that the PDF in the stationary state is sufficiently small, say, 10^{-3} , as determined from the asymptotic form (64).

In order to find a discrete time and position expression for the fractional Riesz derivative in Eq. (130), we employ the Grünwald–Letnikov scheme [110–112], whence we obtain

$$\bar{D}_{j,n} = -\frac{1}{2(\Delta x)^\alpha \cos(\pi\alpha/2)} \sum_{q=0}^J \xi_q [P_{j+1-q,n} + P_{j-1+q,n}] \tag{133}$$

where

$$\xi_q = (-1)^q \binom{\alpha}{q} \tag{134}$$

with

$$\binom{\alpha}{q} = \begin{cases} \alpha(\alpha-1)\dots(\alpha-q+1)/q!, & q > 0 \\ 1, & q < 0 \end{cases} \tag{135}$$

and $1 < \alpha \leq 2$. Note that in the limiting case $\alpha = 2$ only three coefficients differ from zero, namely, $\xi_0 = 1$, $\xi_1 = -2$, and $\xi_2 = 1$, corresponding to the

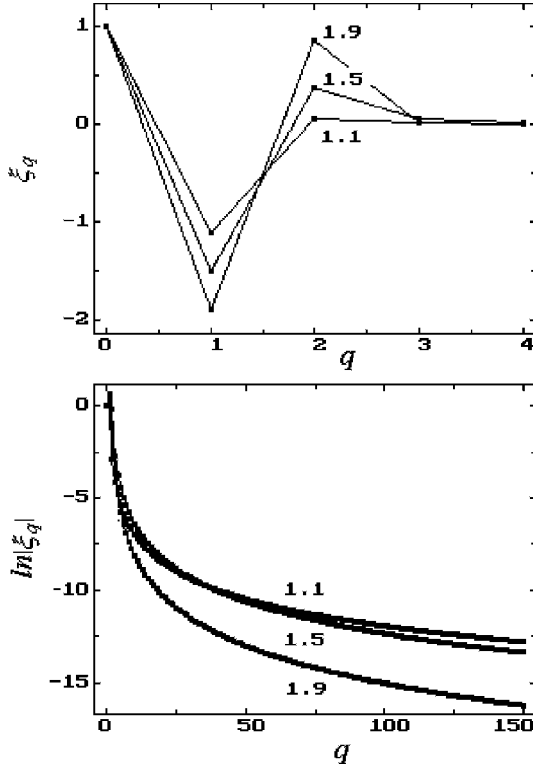


Figure 25. Coefficients ξ_q in Grünwald-Letnikov approximation for different values of the Lévy index $\alpha = 1.9, 1.5,$ and 1.1 .

standard three-point difference scheme for the second order derivative, $d^2g(x_j)/dx^2 \approx (g_{j+1} - 2g_j + g_{j-1})/(\Delta x)^2$. In Fig. 25, we demonstrate that with decreasing α , an increasing number of coefficients contribute significantly to the sum in Eq. (133). This becomes particularly clear in the logarithmic representation in the bottom plot of Fig. 25. We note that the condition

$$\mu \equiv \Delta t / (\Delta x)^\alpha < 0.5 \tag{136}$$

is needed to ensure the numerical stability of the discretisation scheme. In our numerical evaluation, we use $\Delta x = 10^{-3}$, and therefore the associated time increment $\Delta t \sim 10^{-5} \dots 10^{-6}$, depending on the actual value of α . The initial condition for Eq. (131) is $P_{0,0} = 1/\Delta x$.

In Fig. 26, the time evolution of the PDF is shown together with the evolution of the force and diffusion components defined by Eqs. (129) and (130),

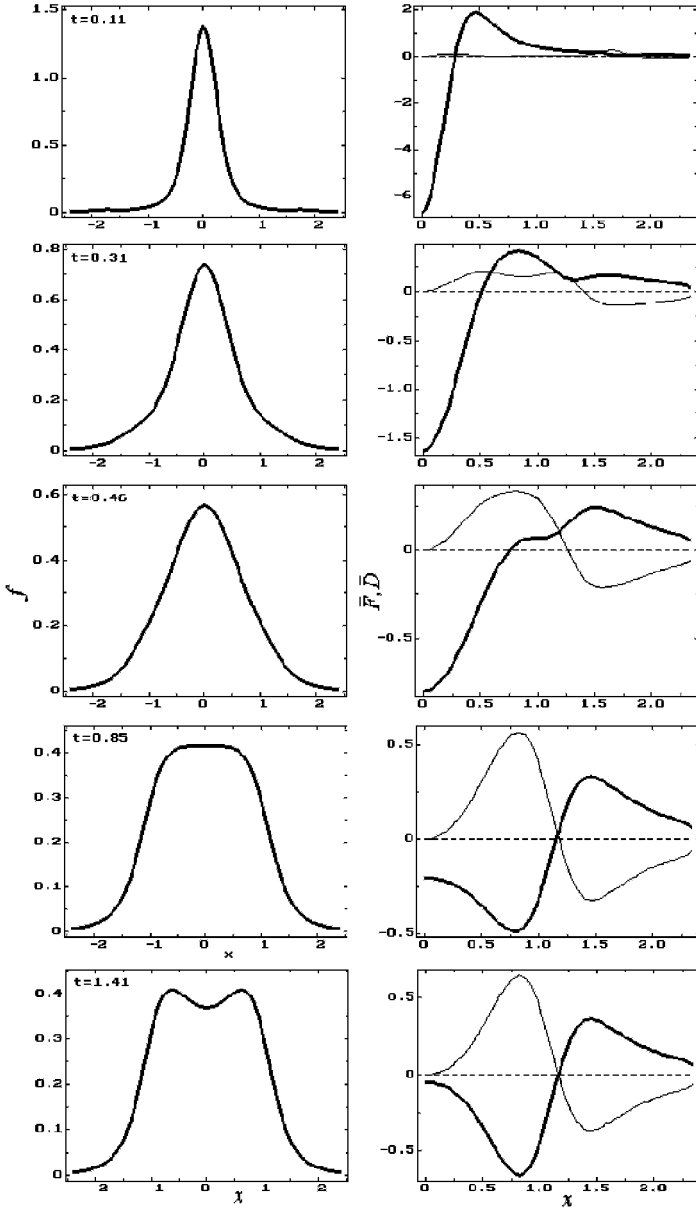


Figure 26. Further details of the Grünwald–Letnikov scheme. *Left:* Time evolution of the PDF as obtained by numerical solution of Eq. (131) at $c = 4$ and $\alpha = 1.2$. *Right:* Time evolution of the diffusion component (130) (thick lines), and of the force term (129) (thin lines).

respectively. Accordingly, at the initial stage of the relaxation process, the diffusion component prevails. The force term grows with time, until in the stationary state $\bar{F} \rightarrow -\bar{D}$. This is particularly visible in the bottom right part of Fig. 26, which corresponds to the stationary bimodal state shown to the left.

B. Numerical Solution of the Langevin Equation [Eq. (25)]

An alternative way to obtain the PDF is to sample the trajectories determined by the Langevin equation [Eq. (25)]. To this end, Eq. (37) is discretized in time according to

$$x_{n+1} = x_n + F(x_n)\Delta t + (\Delta t)^{1/\alpha}\Gamma_\alpha(n\Delta t) \quad (137)$$

with $t_n = n\Delta t$ for $n = 0, 1, 2, \dots$, and where $F(x_n)$ is the dimensionless force field at position x_n . The sequence $\{\Gamma_\alpha(n\Delta t)\}$ is a discrete-time approximation of a white Lévy noise of index α with a unit scale parameter. That is, the sequence of independent random variables possessing the characteristic function $\hat{p} = \exp(-|k|^\alpha)$. To generate this sequence $\{\Gamma_\alpha(n\Delta t)\}$, we have used the method outlined in Ref. 113.

References

1. T. L. Carus, *De rerum natura* (50 BC), *On the Nature of Things*, Harvard University Press, Cambridge, MA, 1975.
2. J. Ingenhousz, *Nouvelles expériences et observations sur divers objets de physique*, T. Barrois le jeune, Paris, 1785.
3. R. Brown, *Philos. Mag.* **4**, 161; (1828); *Ann. Phys. Chem.* **14**, 294; (1828).
4. A. Einstein, *Ann. Phys.* **17**, 549 (1905); *ibid.* **19**, 371 (1906); R. Fürth, Ed., *Albert Einstein—Investigations on the Theory of the Brownian Movement*, Dover, New York, 1956. (Einstein actually introduced the name “Brownian motion,” although he did not have access to Brown’s original work.)
5. J. Perrin, *Comptes Rendus (Paris)* **146**, 967 (1908); *Ann. Chim. Phys. VIII* **18**, 5 (1909).
6. A. Fick, *Ann. Phys. (Leipzig)* **94**, 59 (1855).
7. A. Westgren, *Z. Phys. Chem.* **83**, 151 (1913); *ibid.* **89**, 63 (1914); *Arch. Mat. Astr. Fysik* **11**, 00 (1916); *Z. Anorg. Chem.* **93**, 231 (1915); *ibid.* **95**, 39 (1916).
8. E. Kappler, *Ann. Phys. (Leipzig)* **11**, 233 (1931).
9. S. Chandrasekhar, *Rev. Mod. Phys.* **15**, 1 (1943).
10. P. Lévy, *Processus stochastiques et mouvement Brownien*, Gauthier–Villars, Paris, 1965.
11. N. G. van Kampen, *Stochastic Processes in Physics and Chemistry*, North–Holland, Amsterdam, 1981, 2nd ed., 1992, Reprinted 1997.
12. H. Risken, *The Fokker–Planck Equation* 2nd ed., Springer-Verlag, Berlin, 1989.

13. W. T. Coffey, Y. P. Kalmykov, and J. T. Waldron, *The Langevin Equation*, World Scientific, Singapore, 1996; 2nd ed., 2004.
14. B. D. Hughes, *Random Walks and Random Environments*, Vol. 1: *Random Walks*, Oxford University Press, Oxford, 1995. Note that Hughes coins the term “leapers” for Lévy flights.
15. S. Havlin and D. Ben-Avraham, *Adv. Phys.* **36**, 695 (1987).
16. J.-P. Bouchaud and A. Georges, *Phys. Rep.* **88**, 127 (1990).
17. G. Pfister and H. Scher, *Phys. Rev. B* **15**, 2062 (1977).
18. H. Scher, G. Margolin, R. Metzler, J. Klafter, and B. Berkowitz, *Geophys. Res. Lett.* **29**, 1061 (2002).
19. I. M. Tolic-Nørrelykke, E.-L. Munteanu, G. Thon, L. Oddershede, and K. Berg-Sørensen, *Phys. Rev. Lett.* **93**, 078102 (2004).
20. R. Metzler and J. Klafter, *J. Phys. A* **37**, R161 (2004).
21. E. W. Montroll and G. H. Weiss, *J. Math. Phys.* **6**, 167 (1965).
22. H. Scher and M. Lax, *Phys. Rev.* **137**, 4491 (1973).
23. H. Scher and E. W. Montroll, *Phys. Rev. B* **12**, 2455 (1975).
24. R. Metzler and J. Klafter, *J. Phys. Chem. B* **104**, 3851 (2000).
25. R. Metzler and J. Klafter, *Phys. Rev. E* **61**, 6308 (2000).
26. A. Caspi, R. Granek, and M. Elbaum, *Phys. Rev. Lett.* **85**, 5655 (2000).
27. E. R. Weeks and H. L. Swinney, *Phys. Rev. E* **57**, 4915 (1998).
28. R. Metzler and J. Klafter, *Europhys. Lett.* **51**, 492 (2000).
29. A. J. Dammers and M.-O. Coppens, in *Proceedings of the 7th World Congress on Chemical Engineering, Glasgow, Scotland, 2005*.
30. S. Russ, S. Zschiegner, A. Bunde, and J. Kärger, *Phys. Rev. E* **72**, 030101(R) (2005).
31. P. Levitz, *Europhys. Lett.* **39**, 593 (1997).
32. G. H. Weiss, *Aspects and Applications of the Random Walk*, North-Holland, Amsterdam, 1994.
33. P. Lévy, *Théorie de l'addition des variables aléatoires*, Gauthier-Villars, Paris, 1954.
34. B. V. Gnedenko and A. N. Kolmogorov, *Limit Distributions for Sums of Random Variables* Addison-Wesley, Reading MA, 1954.
35. M. F. Shlesinger, G. M. Zaslavsky, and J. Klafter, *Nature* **363**, 31 (1993).
36. J. Klafter, M. F. Shlesinger and G. Zumofen, *Phys. Today* **49**(2), 33 (1996).
37. M. Levandowsky, B. S. White, and F. L. Schuster, *Acta Protozool.* **36**, 237 (1997).
38. R. P. D. Atkinson, C. J. Rhodes, D. W. Macdonald, and R. M. Anderson, *OIKOS* **98**, 134 (2002).
39. G. M. Viswanathan, V. Afanasyev, S. V. Buldyrev, E. J. Murphy, P. A. Prince, and H. E. Stanley, *Nature* **381**, 413 (1996).
40. G. M. Viswanathan, S. V. Buldyrev, S. Havlin, M. G. E. da Luz, M. P. Raposo, and H. E. Stanley, *Nature* **401**, 911 (1999).
41. G. Ramos-Fernandez, J. L. Mateos, O. Miramontes, G. Cocho, H. Larralde, and B. Ayala-Orozco, *Behav. Ecol. Sociobiol.* **55**, 223 (2003).
42. D. A. Benson, R. Schumer, M. M. Meerschart, and S. W. Wheatcraft, *Transp. Porous Media* **42**, 211 (2001).
43. A. V. Chechkin, V. Y. Gonchar, and M. Szydlowsky, *Phys. Plasma* **9**, 78 (2002).
44. H. Katori, S. Schlipf, and H. Walther, *Phys. Rev. Lett.* **79**, 2221 (1997)

45. J. Klafter, A. Blumen, and M. F. Shlesinger, *Phys. Rev. A* **35**, 3081 (1987).
46. R. Metzler and J. Klafter, *Phys. Rep.* **339**, 1 (2000).
47. M. F. Shlesinger, J. Klafter, and Y. M. Wong, *J. Stat. Phys.* **27**, 499 (1982).
48. I. M. Sokolov and R. Metzler, *Phys. Rev. E* **67**, 010101(R) (2003).
49. J. Klafter and R. Silbey, *Phys. Rev. Lett.* **44**, 55 (1980).
50. R. Metzler, *Eur. Phys. J. B* **19**, 249 (2001).
51. *Phys. Rev. E* **62**, 6233 (2000).
52. R. Metzler, E. Barkai, and J. Klafter, *Europhys. Lett.* **46**, 431 (1999).
53. A. Compte, *Phys. Rev. E* **53**, 4191 (1996).
54. H. C. Fogedby, *Phys. Rev. Lett.* **73**, 2517 (1994).
55. H. C. Fogedby, *Phys. Rev. E* **58**, 1690 (1998).
56. F. Pešekis, *Phys. Rev. A* **36**, 892 (1987).
57. S. Jespersen, R. Metzler and H. C. Fogedby, *Phys. Rev. E* **59**, 2736 (1999).
58. R. Metzler, E. Barkai, and J. Klafter, *Phys. Rev. Lett.* **82**, 3563 (1999).
59. V. Seshadri and B. J. West, *Proc. Natl. Acad. Sci. USA* **79**, 4501 (1982); B. J. West and V. Seshadri, *Physica* **113A**, 203 (1982).
60. A. Chechkin, V. Gonchar, J. Klafter, R. Metzler and L. Tanatarov, *Chem. Phys.* **284**, 233 (2002).
61. F. Mainardi, Yu. Luchko, and G. Pagnini, *Fract. Calc. Appl. Anal.* **4**, 153 (2001).
62. S. G. Samko, A. A. Kilbas and O. I. Marichev, *Fractional Integrals and Derivatives, Theory and Applications*, Gordon and Breach, New York, 1993.
63. A. V. Chechkin, J. Klafter, V. Y. Gonchar, R. Metzler, and L. V. Tanatarov, *Phys. Rev. E* **67** 010102(R) (2003).
64. A. V. Chechkin, V. Y. Gonchar, J. Klafter, R. Metzler, and L. V. Tanatarov, *J. Stat. Phys.* **115**, 1505 (2004).
65. I. Eliazar and J. Klafter, *J. Stat. Phys.* **111**, 739 (2003).
66. R. Balescu, *Equilibrium and Nonequilibrium Statistical Mechanics*, Vol. II, Wiley, New York, 1975.
67. P. Benetatos, T. Munk, and E. Frey, *Phys. Rev. E* **72**, 030801(R) (2005).
68. E. Schrödinger, *Phys. Z.* **16**, 289 (1915).
69. W. Feller, *An Introduction to Probability Theory and Its Applications*, Wiley, New York, 1968.
70. S. Redner, *A guide to First-Passage Processes*, Cambridge University Press, Cambridge, UK, 2001.
71. E. W. Montroll and B. J. West, in *Fluctuation Phenomena*, E. W. Montroll and J. L. eds. Lebowitz, North-Holland, Amsterdam, 1976.
72. M. Gitterman, *Phys. Rev. E* **62**, 6065 (2000); compare to the comment by S. B. Yuste and K. Lindenberg, *Phys. Rev. E* **69**, 033101 (2004).
73. E. Sparre Andersen, *Math. Scand.* **1**, 263 (1953).
74. E. Sparre Andersen, *Math. Scand.* **2**, 195 (1954).
75. U. Frisch and H. Frisch, in *Lévy flights and related topics in physics*, Lecture Notes in Physics, Vol. 450, edited by M. F. Shlesinger, G. M. Zaslavsky, and U. Frisch (Springer-Verlag, Berlin, 1995).
76. G. Zumofen and J. Klafter, *Phys. Rev. E* **51** 2805 (1995).

77. A. V. Chechkin, R. Metzler, J. Klafter, V. Y. Gonchar, and L. V. Tanatarov, *J. Phys. A* **36**, L537 (2003).
78. A. M. Mathai and R. K. Saxena, *The H-Function with Applications in Statistics and Other Disciplines*, Wiley Eastern Ltd., New Delhi 1978.
79. W. G. Glöckle and T. F. Nonnenmacher, *J. Stat. Phys.* **71**, 755 (1993).
80. H. Scher, G. Margolin, R. Metzler, J. Klafter, and B. Berkowitz, *Geophys. Res. Lett.* **29**, 10.1029/2001GL014123 (2002).
81. R. Metzler and J. Klafter, *Biophys. J.* **85**, 2776 (2003).
82. F. D. Gakhov, *Boundary Value Problems*, Pergamon Press, Oxford, 1966.
83. H. A. Kramers, *Physica* **7**, 284 (1940).
84. P. Hänggi, P. Talkner, and M. Bokrovec, *Rev. Mod. Phys.* **62**, 251 (1990).
85. R. Metzler and J. Klafter, *Chem. Phys. Lett.* **321**, 238 (2000).
86. A. V. Chechkin, V. Y. Gonchar, J. Klafter, and R. Metzler, *Europhys. Lett.*, **00**, 000 (2005).
87. P. D. Ditlevsen, *Geophys. Res. Lett.* **26**, 1441 (1999).
88. J. Fajans and A. Schmidt, *Nucl. Instrum. & Methods in Phys. Res. A* **521**, 318 (2004).
89. P. Hänggi, T. J. Mroczkowski, F. Moss, and P. V. E. McClintock, *Phys. Rev. A* **32**, 695 (1985).
90. A. V. Chechkin and V. Y. Gonchar, *Physica A* **27**, 312 (2000)
91. P. D. Ditlevsen, *Phys. Rev. E* **60**, 172 (1999)
92. Y. L. Klimontovich, *Statistical Theory of Open Systems*, Vol. 1, Kluwer Academic Publishers, Dordrecht, 1995.
93. G. Zumofen and J. Klafter, *Chem. Phys. Lett.* **219**, 303 (1994).
94. I. M. Sokolov, J. Mai, and A. Blumen, *Phys. Rev. Lett.* **79**, 857 (1997).
95. G. Cattaneo, *Atti. Sem. Mat. Fis. Univ. Modena* **3**, 83 (1948).
96. P. C. de Jagher, *Physica A* **101**, 629 (1980).
97. G. Zumofen and J. Klafter, *Phys. Rev. E* **47**, 851 (1993).
98. M. F. Shlesinger, J. Klafter, and Y. M. Wong, *J. Stat. Phys.* **27**, 499 (1982).
99. R. N. Mantegna and H. E. Stanley, *Phys. Rev. Lett.* **73**, 2946 (1994).
100. I. M. Sokolov, A. V. Chechkin, and J. Klafter, *Physica A* **336**, 245 (2004).
101. N. N. Bogoliubov and Y. A. Mitropolsky, *Asymptotic Methods in the Theory of Non-linear oscillations*, Hindustan Publishing Corp., Delhi, distributed by Gordon & Breach, New York, 1961.
102. H. Davis, *Introduction to Nonlinear Differential and Integral Equations*, Dover Publications, New York, 1962.
103. A. A. Andronow, C. E. Chaikin, and S. Lefschetz S., *Theory of Oscillations*, Princeton University Press, Princeton, NJ, 1949.
104. L. D. Landau and E. M. Lifshitz, *Course of Theoretical Physics*, Vol. 6: *Fluid Mechanics*, Pergamon Press, London, 1966.
105. Y. L. Klimontovich, *Turbulent Motion and the Structure of Chaos: A New Approach to the Statistical Theory of Open Systems*, Kluwer, Dordrecht, NL, 1992.
106. J. M. Halley, S. Hartley, A. S. Kallimanis, W. E. Kunin, J. J. Lennon, and S. P. Sgardelis, *Ecology Lett.* **7**, 254 (2004).
107. E. Frey and K. Kroy, *Ann. Phys.* **14**, 20 (2005).

108. P. Hänggi and F. Marchesoni, *Chaos* **15**, 026101 (2005).
109. J. Klafter and I.M. Sokolov, *Phys. World* **18**(8), 29 (2005).
110. I. Podlubny, *Fractional Differential Equations*, Academic Press, San Diego, CA, 1998.
111. R. Gorenflo, in *Fractals and fractional calculus in continuum mechanics* A. Carpinteri and F. Mainardi, eds., Springer, Wien, 1997.
112. R. Gorenflo, F. Mainardi, D. Moretti, G. Pagnini, and P. Paradisi, *Chem. Phys.* **284**, 521 (2002).
113. A. V. Chechkin and V. Y. Gonchar, *Physica A* **27**, 312 (2000).